Glass Transition and Relaxation: Insights from Calorimetry

Guo, Xiaoju

Publication date:
2012

Document Version
Early version, also known as pre-print

Glass Transition and Relaxation: Insights from Calorimetry

Xiaoju Guo

Section of Chemistry
Aalborg University
Ph.D. Dissertation, 2012

ISBN : 978-87-90033-96-5

AALBORG UNIVERSITY

Ph. D. Dissertation

Glass Transition and Relaxation: Insights from Calorimetry

By
Xiaoju Guo

Section of Chemistry
Department of Biotechnology, Chemistry,
and Environmental Engineering
Aalborg University, Denmark

Date of Defense
October 25th, 2012

Assessment Committee

Morten L. Christensen
Associate Professor
Aalborg University,
Denmark

Prabhat Gupta
Professor
Ohio State University,
USA

Punit Boolchand
Professor
University of Cincinnati,
USA

Supervisor
Yuanzheng Yue
Professor
Aalborg University,
Denmark

John C. Mauro
Research Associate
Corning Incorporated,
USA

Preface and Acknowledgement

This thesis is submitted to the Faculty of Engineering, Science and Medicine in partial fulfillment of the requirement for obtaining the Ph. D. degree. The Ph. D. study was carried out full time from April 1st 2009 to September 30th 2010 and part time from October 1st, 2010 to July 15th, 2012. The full time part was done at the Section of Chemistry at Aalborg University with the financial support by FTP, and the part time part was done in Corning Incorporated as a full time employee in Corning Incorporated.

I highly appreciate my supervisor Yuanzheng Yue for his dedicated supervision and great help throughout the whole project. This is a great topic for a beginner to get deeper understanding of glass science. I look forward to working close with you and continue collaboration for the fascinating glass scientific projects in the future. In addition, I am grateful to Yuanzheng to give me the chance to do the internship in Corning at summer of 2010, the right time when I got current permanent position as a development scientist in Corning Incorporated. My great thankfulness also goes to my co-supervisor, John C. Mauro in Corning Incorporated who has had great impact on the scientific work I have accomplished during the Ph. D. time, with especially close supervision while I was working part time for the degree as a full time employee at Corning. I would also like to take this opportunity to express my acknowledgements to my supervisor, Ronald L. Stewart at Corning, for providing this great position for me to continue on exciting scientific research on glass science. I am grateful to Mette Solvang from Rockwool International A/S for providing the basalt fiber samples.

I take great pleasure in acknowledging my supervisor for my first Ph. D, Yongjun Tian from Yanshan University in China, who made the recommendation for me to come to Denmark for this degree and gave me great supervision for me to become an independent scientist.

I would like to thank my colleagues in the inorganic amorphous materials group for fruitful scientific discussions. The names that should be specially mentioned are Ralf Keding, Morten M. Smedskjaer, Martin Jensen, Qiuju Zheng, and Mette Moesgaard. My special thanks goes to Yuqing Zhang, who helped on developing the C++ version of the model. Finally I would like to thank my husband for all his support throughout the project.

Abstract

Glass transition and glass relaxation have been known as two of the most difficult problems in the field of condensed matter physics. It is well known that glass transition is a dynamic property governed by composition and the observation window. One of the remaining questions of glass transition is how it is affected by the glass structure itself. Glass relaxation is a more complicated function not only of composition and observation time window but also the thermal history that the glass has experienced from the equilibrium state.

The glass transition temperature and relaxation rate are dependent on the properties under consideration. One of the most useful techniques in probing glass transition is differential scanning calorimetry (DSC). The current work is based on experiments and simulations of the glass heat capacity as a function of temperature obtained from DSC upscans. In this thesis we prove that the glass transition is irrelevant to the glass structure itself in the DSC upscan from heat capacity data and simulated reversing heat flow in temperature modulated differential scanning calorimetry (TMDSC).

Relaxation rate is not only a function of composition and temperature, but also a function of glass structure, which is controlled by the thermal history as well as composition. In order to study the effect of glass structure on relaxation, information on glass structure should be considered. Fictive temperature has been used to describe the thermal history as one single number. We have noticed that the approaches proposed by Moynihan and Yue cannot be used to accurately describe the heat capacity curves of some of our annealed hyperquenched glass fibers. Based on the identical definition of fictive temperature from Moynihan as the two techniques stated above, a unified approach will be proposed for the fictive temperature determination for glasses that have experienced arbitrary thermal history, which is a combination of Moynihan's and Yue's techniques.

In the study of glass relaxation, we focus on the property of enthalpy, which is determined from DSC. In order to understand the relaxation mechanism of glasses far from equilibrium, systematic annealing of basalt fibers formed by the hyperquenching method were carried out at temperatures from $0.6T_g$ to $0.9T_g$ for various durations. The enthalpy recovery of the annealed hyperquenched fibers reveals that secondary relaxation is fully decoupled from primary relaxation when the fictive temperature is in the range of 930 K to 1200 K and secondary relaxation governs the enthalpy recovery. Our results also show that a distribution of fictive temperatures is required to capture the broad distribution of relaxation times other than a single fictive temperature value. The distribution of the fictive temperature represents the thermal history.

In addition, the variability of the stretching exponent with fictive temperature explains why the composite relaxation function performs better than the normal KWW function where tretching exponent is expressed as a constant. The simulated heat capacity curves of basalt fiber with three distinct thermal histories--slowly cooled, hyperquenched, and annealed hyperquenched-- reveal that the composite relaxation function can capture the onset temperature of the pre-T_g endotherm peak and the fast increasing overshoot endotherm peak in the glass transition range. The enthalpy relaxation distribution in the middle temperature range (about $0.7T_g$ to $0.9T_g$) is also smoother compared to the KWW function.

Table of Contents

Preface and Acknowledgement I

Abstract III

1. Introduction 1

1.1 Background 2
1.2 Objectives 4
1.3 Thesis Content 5

2. Modeling setup 7

2.1 Relaxation of glass forming liquids 7
2.2 Relaxation of the non-equilibrium state 9
2.3 Stretching exponent in the model 10
2.4 Modeling process for TMDSC 11

3. Dependence of glass transition on glass structure 13

3.1 Glass transition of basaltic fibers 13
3.2 TMDSC modeling of Glass transition 16
3.2.1 Heat flow deconvolution in TMDSC 16
3.2.2 Frequency correction for reversing heat flow 18
3.3 Brief summary 23

4. Thermodynamic Glass State 24

4.1 Non-reversing heat flow in TMDSC 24
4.1.1 Frequency correction of non-reversing heat flow 25
4.1.2 Enthalpy recovery from non-reversing heat flow 27
4.2 Thermodynamic glass state determination 28
4.2.1 The limitation of existing approaches 28
4.2.2 Generalized approach 31
4.2.3 Numerical validation of the unified approach 34
4.2.4 Advantage of the unified approach 36
4.3 Brief summary 38

5. Structural relaxation in annealed hyperquenched basaltic glasses 39

5.1 Specific heat measured by DSC 39

5.2 Enthalpy recovery analysis.....43
5.2.1 Isolation of secondary relaxation from primary relaxation.....43
5.2.2 Enthalpy relaxation time and stretching exponent.....45
5.3 Brief summary.....49
6. Heat capacity modeling from composite relaxation function.51
6.1 A composite relaxation function.....51
6.2 Heat capacity simulation of fresh and annealed hyperquenched fiber.....53
6.2.1 The Stretching exponent.....53
6.2.2 Determination of all other parameters.....54
6.2.3 Heat capacity modeling for hyperquenched fiber.....55
6.2.4 Enthalpy recovery of the annealed hyperquenched fibers.....59
6.3 Brief summary.....61
7. Summary and perspectives.....62
References.....64

1. Introduction

The initial plan for this Ph.D. project was to conduct systematic studies of enthalpy relaxation in thin glass fibers of different compositions. The fibers are cooled at very high cooling rates (10^5 to 10^6 K/s) during their drawing process, i.e., they are "hyperquenched", and hence are far from equilibrium state. As it is known, none of the existing models can accurately describe the enthalpy relaxation of the hyperquenched glasses. Thus it was planned to develop a model with physical meanings in the frame of this project. However, later on we realized that owing to so many unanswered questions about relaxation of hyperquenched (HQ) glass the original goal was too ambitious. Therefore, the focus of the current project was changed to tackle some basic problems related to glass transition and relaxation.

Glass is a non-equilibrium, non-crystalline solid formed when a (supercooled) liquid is cooled faster than a critical cooling rate to avoid crystallization (Debenedetti et al. 2001, and Varshneya 2007). Dynamically, the vitrification begins when the cooling rate at a given temperature is too fast for the viscous liquid relaxation to follow. On the other hand, the glass will be transformed to the supercooled liquid upon heating. Both of the transformations in cooling and heating are all defined as glass transition in glass science. The temperature range of glass transition will depend on the comparison of observation time scale in cooling/heating and the relaxation time of the system itself. This relaxation time includes not only the relaxation of liquid but also relaxation of non-equilibrium glass state. The reason to separate glass relaxation from liquid relaxation is that glass and liquid relaxation are fundamentally different.

Glass transition and glass relaxation are fundamentally different behaviors, but cannot be treated independently. Phenomenologically, the thermal expansion, heat capacity, and many other properties of inorganic glasses show a relatively sudden change at the glass transition temperature, although it is not a second-order phase transition. Thus, glass transition is easier to be observed as a dynamic

phenomenon. Like many other problems in glass science, the study of glass transition has been difficult because of the non-equilibrium, non-crystalline structure of glass, and very small structure changes in glass transition (Phillips 1982). The glass transition is the key to understanding the nature of glass. The current project attempts to provide some insights into both glass transition and relaxation.

1.1 Background

Since a sudden change in heat capacity or in thermal expansion occurs during glass transition, the temperature regime of glass transition can normally be probed by measuring the energy release on heating in a differential scanning calorimetry (DSC) or the volume change on heating in a dilatometry. In order to characterize the glass transition range, a single glass transition temperature (T_g) is widely used as a characteristic value of the liquid/glass system. T_g strongly depends on the heating/cooling rate. Only when the cooling rate during glass formation and the heating rate in the DSC measurement are defined, T_g can be used as the standard thermodynamic value and can be compared among different glasses. As is known, the thermodynamic T_g value is correlated to the dynamic one. Conventionally the temperature at the equilibrium viscosity at 10^{12} Pa-s is defined as the dynamic T_g (Alba et al. 1990, Angell 1991, Angell et al. 2000). In order to standardize the concept of thermodynamic T_g, Yue (Yue, 2008) has performed systematic study of the data in literature, and then suggested that the rate of 10 K/min should be applied for both the prior DSC downscan and the subsequent upscan in order to obtained the standard thermodynamic T_g values that equal to the dynamic ones, i.e., the temperature at 10^{12} Pa s. In the molecule and polymer glass systems, 20 K/min (Wang et al, 2008) is used as the standard heating rate in T_g measurement. The cooling rate is the key factor in determining the glass structure. Now several questions arise. Should we expect different T_g values for glasses made by different cooling rate? If so, only one heating rate is not sufficient to get a standard T_g, a standardized cooling rate for forming the glass is also required (Wang et al, 2008). How much can

the cooling rate affect T_g? How should we determine T_g of the glass system. Is T_g an intrinsic characteristic thermodynamic value for the onset of the glass transition process?

After a glass is formed and kept at a temperature with no observable relaxation, the glass stays in one particular state (having some particular structure). Different from equilibrium/metastable liquid, the energetics and structure of the glassy state are not only functions of composition, temperature, and pressure but also on the thermal history experienced. Thermal history is a more complicated factor comparing to temperature or pressure, and it is a function of temperature and time since the equilibrium liquid state where the glass is from. Great effort has been made to simplify this complicated variable to describe the macroscopic state of a glass. The glass state was described in terms of an equilibrium (metastable) liquid state corresponding to a special temperature (Tool et al. 1931). The special temperature of the liquid was then defined as "effective temperature" or "fictive temperature (T_f)" (Tool 1946). The latter is more commonly used in literature. Narayanaswamy (Narayanaswamy 1971) introduced additional order of parameters in the form of multiple fictive temperatures. An alternative definition of fictive temperature was proposed by Moynihan et al., i.e., T_f is defined as "simply the structural contribution to the value of the macroscopic property of interest expressed in temperature units" (Moynihan et al 1976 & Moynihan 1993). This definition is based on the macroscopic thermodynamics of glass. It simplified the thermal history/fictive temperature as a variable from a function of temperature and time to a single number in relation to a specific property. As such a useful variable, the calculation of fictive temperature is very important in terms of description of the glass state. However, the measurement and calculation of T_f for glasses having different thermal histories are complicated by structural relaxation during measurement. Is there a unified approach in the fictive temperature determination?

As stated above, glass transition is accompanied by liquid and glass relaxation. But relaxation is a general phenomenon since it occurs not only in the glass transition region, but also beyond that

region. In the molecule and polymer glass fields, relaxation time of liquid and glass could be probed by dielectric constant measurement. Then the dielectric constant spectrum could be analyzed by Cole-Cole function (Cole and Cole 1941 and 1942), Cole-Davidson (Davidson and Cole 1950 &1951) or Havriliak-Negami (Havriliak & Negami 1967) functions. However, the relaxation study of silicate glasses/liquids has to be performed in some alternative way because of the high temperature range. The general approach to study the inorganic systems is viscometry, by which the shear viscosity can be measured as a function of temperature. The average structural relaxation time can be calculated from viscosity data through the Maxwell relation (Maxwell 1867). The relaxation time of the nonequilibrium glass state has received considerably less attention, primarily due to the exceedingly long relaxation times involved at temperatures below the glass transition. The nonequilibrium relaxation occurring in the sub-T_g annealing process is a function of temperature, pressure, and thermal history which makes the theoretical description of the nonequilibrium viscosity more complicated and challenging. On the other hand, enthalpy recovery in sub-T_g annealing has been used as another tool for the study of nonequilibrium relaxation. Hyperquenched glass fibers proved to be the object of the enthalpy recovery study due to the far from equilibrium feature, which gives detailed information on the enthalpy relaxation, especially by performing sub-T_g annealing (Yue et al 2002 & 2004, Hornboell et al 2008 & 2010). The hyperquenched fibers investigated in the current project were provided by Rockwool International A/S in Denmark.

1.2 Objectives

The present Ph. D. thesis is focused on the following objectives:

1. Reveal that the cooling rate used during glass forming does not affect T_g in the post-forming glass transition measurement in both modeling and experiment.

2. Establish a unified approach for determining the fictive temperature of a glass that experienced any arbitrary thermal history.

3. Probe the structural relaxation in the sub-T_g annealing process of hyperquenched basaltic fibers by calorimetry.

The above listed three topics are all related to the fundamental knowledge of glass science; here we try to clarify some unclear or misunderstanding concepts or the misapplication of these concepts in the glass science community.

1.3 Thesis Content

The present thesis will be organized as a plurality, including an introductory overview followed by three peer-reviewed journal papers. Modeling as a powerful tool is used in the TMDSC study and establish of the unified approach for fictive temperature determination, chapter 2 will give an overview of the approach used in the modeling with a simple comparison with other existing models. Also in chapter 2, the modeling process for TMDSC will be presented. Then it will be followed by the insights to the glass transition from experiments and modeling, the unified approach for fictive temperature determination revealing that fictive temperature is a thermodynamic property which could represent the glass state, and the experimental structural relaxation in the hyperquenched basaltic fibers. The last topic is an advantage of the composite relaxation function comparing with KWW function where the hyperquenched and annealed basaltic fibers will be discussed as an example. Finally, the three publications are attached at the end of the thesis.

The three peer-reviewed journal papers are listed here:

I. Xiaoju Guo, Marcel Potuzak, John C. Mauro, Douglas C. Allan, T. J. Kiczenski, Yuanzheng Yue, “Unified approach for determining the enthalpic fictive temperature of

glasses with arbitrary thermal history", J. Non-Cryst. Solids, 357 (2011) 3230-3236

II. Xiaoju Guo, John C. Mauro, Marcel Potuzak, Yuanzheng Yue, "Structural relaxation in annealed hyperquenched basaltic glasses: Insights from calorimetry", J. Non-Cryst. Solids, 358 (2012)1356-1361

III. Xiaoju Guo, John C. Mauro, Douglas C. Allan, Yuanzheng Yue, "On the frequency correction in the temperature-modulated differential scanning calorimetry of glass transition and relaxation behavior", J. Non-Cryst. Solids, 358 (2012)1710-1715

2. Modeling setup

The modeling of relaxation in this thesis includes the following steps: 1) the simulation starts from the equilibrium liquid state; 2) the equilibrium relaxation is calculated by Mauro-Yue-Ellison-Gupta-Allan (MYEGA) equation (Mauro et al., 2009a); 3) the non-equilibrium relaxation is described by Mauro-Allan-Potuzak (MAP) model (Mauro et al. 2009b).

2.1 Relaxation of glass forming liquids

Several empirical, semi-empirical, and phenomenological models have been proposed in literature to describe the temperature dependence of the equilibrium viscosity (or relaxation time).

The most popular viscosity model for equilibrium or metastable liquid state is the Vogel-Fulcher-Tammann (VFT) equation (Vogel, 1921, Fulcher, 1925, and Tammann and Hesse, 1926):

$$\log_{10}\eta(T,x) = \log_{10}\eta_{\infty}(x) + \frac{A(x)}{T - T_0(x)}, \qquad (2\text{-}1)$$

where T is temperature, x is composition, η_{∞} is the high temperature limit of viscosity, A and T_0 are fitting parameters.

Avramov-Milchev (AM) equation is another three-parameter viscosity model (Avramov and Milchev, 1988):

$$\log_{10}\eta(T,x) = \log_{10}\eta_{\infty}(x) + \left(\frac{\tau(x)}{T}\right)^{\alpha(x)}, \qquad (2\text{-}2)$$

where η_{∞}, τ, and α are fitting parameters.

Among all empirical models, the Adam-Gibbs equation (Adam and Gibbs, 1965) establishes relation between dynamic viscosity and thermodynamic configurational entropy of the liquid, $S_c(T,x)$:

$$\log_{10}\eta(T,x) = \log_{10}\eta_{\infty}(x) + \frac{B(x)}{TS_c(T,x)}, \qquad (2\text{-}3)$$

where B(x) is an effective activation barrier, which is normally taken as a fitting parameter.

Recently, a new model was proposed by Mauro et al. (Mauro et al, 2009a) where they calculated the configurational entropy in the Adam-Gibbs equation in terms of the topological degrees of the freedom per atom in the energy landscape theory. Finally, they simplified the model to another three-parameter model, called the MYEGA model:

$$\log_{10}\eta(T,x) = \log_{10}\eta_{\infty}(x) + \frac{K(x)}{T}\exp\left(\frac{C(x)}{T}\right), \qquad (2\text{-}4)$$

where η_{∞}, $K(x)$, and $C(x)$ are fitting parameters. Lunkenheimer et al. (Lunkenheimer et al 2010) performed a detailed study of the temperature dependence of α-relaxation times of 13 glass formers by fitting the data by VFT and MYEGA, where the MYEGA was declared "to be a good alternative to the VFT equation". The overall performance of MYGEA equation compare to VFT equation revealed that MYEGA equation is preferable to other approaches. Thus, MYEGA equation is utilized in our modeling to describe the relaxation time of glass forming liquids.

In order to express the model with more meaningful quantities, the fragility index of liquid and kinetic T_g (viscosity equals 10^{12} Pa-s) are introduced into the equation. Fragility (Angell 1995) is defined as:

$$m(x) = \left.\frac{\partial \log_{10}\eta(T,x)}{\partial\left(T_g(x)/T\right)}\right|_{T=T_g(x)}. \qquad (2\text{-}5)$$

Finally, MYEGA equation can be expressed in the following expression:

$$\log_{10}\eta(T,x) = \log_{10}\eta_{\infty}(x) + \left(12-\log_{10}\eta_{\infty}\right)\frac{T_g}{T}\exp\left[\left(\frac{m}{12-\log_{10}\eta_{\infty}}-1\right)\left(\frac{T_g}{T}-1\right)\right]. \qquad (2\text{-}6)$$

2.2 Relaxation of the non-equilibrium state

When a liquid is cooled from the equilibrium state, the liquid will be out of equilibrium as soon as the glass transition starts. Thus, the glass transition and the glass state are all controlled by the nonequilibrium relaxation process. However, the nonequilibrium relaxation of a glass has received considerably less attention, primarily due to the exceedingly long relaxation times involved at glass transition range and sub-T_g temperatures.

In literature, several models have been proposed to describe the nonequilibrium relaxation, including the theoretical work of Tool-Narayanaswamy (Tool 1946, and Narayanaswamy1971), Mazurin et al (Mazurin et al 1983, and Mazurin 1986, and Priven 2001), Avramov (Avramov 1991), and Mauro-Allan-Potuzak (MAP) (Mauro et al 2009b). To some extent, the Adam-Gibbs equation (Adams and Gibbs 1965) could also be taken as a model for the nonequilibrium relaxation if the configurational entropy of glass state could be determined. Nonequilibrium relaxation has attracted attention of glass scientists for many decades. But the experimental validation of the nonequilibrium relaxation models is challenging considering the long time scale and the fact that nonequilibrium relaxation is a function of temperature and thermal history. Although the thermal history of a glass system has been simplified to fictive temperature in terms of macroscopic properties, the investigation of nonequilibrium relaxation is still difficult.

It has been shown that the MAP model gives better description of the nonequilibrium viscosity over a wide range of temperature and fictive temperature in comparison with other models. Please refer to the reference from Mauro et al (Mauro et al 2009b) for the comparison between different nonequilibrium relaxation models. Here the MAP model which is used in our modeling work is presented as:

$$\log_{10}\eta(T,T_f) = x\log_{10}\eta_{eq}(T_f) + (1-x)\log_{10}\eta_{ne}(T,T_f), \quad (2\text{-}7)$$

where x is the ergodicity parameter, $\eta_{eq}(T_f)$ and $\eta_{ne}(T,T_f)$ are the equilibrium contribution and nonequilibrium viscosities, respectively. The ergodicity parameter x is defined by

$$x = \left(\frac{\min(T,T_f)}{\max(T,T_f)} \right)^p . \tag{2-8}$$

The equilibrium viscosity in equation (2-7) incorporates MYEGA equation. Based on the feature of the nonequilibrium viscosity that the glass will reach isostructure state at low temperature limit, the nonequilibrium viscosity is adopted as

$$\log_{10} \eta_{ne} = \frac{\Delta H}{kT \ln 10} + A - BT_f \tag{2-9}$$

where ΔH, A, and B are constants for a given glass composition and are treated as fitting parameters in the model.

The advantage of the MAP model is that the equilibrium and nonequilibrium viscosity can be described by one single expression. Thus, it is applicable for the whole range of glass transition and relaxation revealing the advantage to be used in modeling of glass transition and relaxation.

2.3 Stretching exponent in the model

It is well known that relaxation in most nonequilibrium glassy systems is manifested as a nonexponential decay. The relaxation behavior follows a stretched exponential function, viz., the Kohlrausch-Williams-Watts (KWW) function (Kohlrausch 1847, Kohlrausch, 1854, and Williams and Watts, 1970):

$$f(t) = \exp\left[-\left(\frac{t}{\tau} \right)^{\beta} \right], \tag{2-10}$$

where t is the laboratory time, τ is the relaxation time of the glass state, and β is the dimensionless stretching exponent. The stretching exponent β is an important parameter for describing the distribution of relaxation times in the glass. According to Macdonald and Phillips

(Macdonald and Phillips, 2005, and Phillips, 1996 & 2006) and Potuzak *et al.* (Potuzak et al 2011), the stretching exponent for structural relaxation of microscopically homogeneous glasses is $3/7 \approx 0.43$.

In the model used for the TMDSC simulation and fictive temperature determination, the stretching exponent is expressed as a Prony series of twelve simple exponential terms for convenience of the numerical solution, which has been described in Scherer's relaxation book (Scherer, 2005).

2.4 Modeling process for TMDSC

The simulated TMDSC experiments are performed for EAGLE XG® glass. All of the parameters needed in the model for EAGLE XG® glass are published in Mauro et al. (Mauro et al, 2009b) The EAGLE XG® glass was made by fusion draw forming process where the glass was cooled very fast, thus the heat flow of the pre-made glass is named as hyperquenched. In the model, the simulated experiment mimics the real glass forming process. Thus, the modeled glass is formed by quenching as a pre-thermal history which is cooled to room temperature, 25 ^{o}C. Then the glass is subjected to two TMDSC upscans with one intermediate downscan. As shown in Fig. 2-1, the starting temperature of the simulated TMDSC scan is 25 ºC. The maximum temperature reached during both upscans is 1000 ºC, which is well above the glass transition temperature of T_g = 735.7 ºC (the temperature where the equilibrium viscosity is 10^{12} Pa-s). The linear heating/cooling rate is 1 ºC/min, and the amplitude of the periodic sinusoidal perturbation is 5 ºC. The modulation frequency is varied from 0.0005 to 0.01 Hz, corresponding to a range of periods from 100 to 2000 s. During the first upscan, this quenched glass is heated to an equilibrium state (1000 ^{o}C) and then cooled back to 25 ^{o}C. A second, identical upscan is then performed for this "rejuvenated" glass.

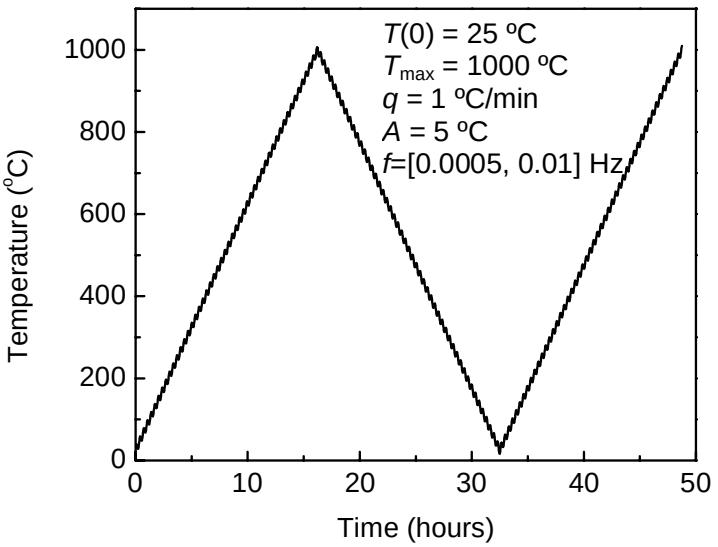

Figure 2-1. Thermal path setting up in TMDSC simulation, the starting temperature 25 ºC, maximum temperature reached at both upscans 1000 ºC, the basic linear heating/cooling rate 1 ºC/min, the amplitude of the periodic sinusoidal perturbation 5 ºC, and modulation frequencies (f) ranged from 0.0005 to 0.01 Hz.

3. Dependence of glass transition on glass structure

As stated in the introduction part, glass transition is far from fully understood. As stated by Nobel Prize winner Philip W. Anderson (Anderson, 1995), the deepest and most interesting unsolved problem in solid state theory is probably the theory of the nature of glass and glass transition. Although the glass transition is under debate concerning whether even it is a phase transition or not, the gradual change of the second order properties such as thermal expansion coefficient and heat capacity in the narrow temperature range is named as a transition.

Many efforts have been devoted to understanding of how the following two factors affect glass transition: 1) the composition of the glass forming system, which is considered as the thermodynamic nature for glass transition; 2) the dynamic heating or cooling rate in the glass to liquid or liquid to glass transition, which finally determines glass transition as a dynamic property. Both factors will alter the glass structure greatly. Different compositions will result in changes of glass network connectivity, thus, affect the glass transition temperature range and glass structure . (Micoulaut and G. G. Naumis, 1999) However, for the same composition, how should we expect the glass structure difference resulted from different cooling rate in glass forming process will affect the glass transition in the post-forming heating process such as in the DSC measurement? Here we will give two examples on this problem both experimentally and theoretically.

3.1 Glass transition of basaltic fibers

The heat capacity curves of fresh hyperquenched (HQ) basaltic fibers, a slow cooled fiber with the same composition and the fibers annealed at 773, 823 and 873 K are shown in Figs. 3-1 (a) to (c), respectively. As for the annealed fibers, a clear pre-endotherm peak appears at temperatures below T_g, an effect that has also been

observed in HQ metallic glasses (Yue et al, 2002a), molecules (Wang et al, 2007), and other oxide glasses (Yue et al, 2002b, Yue and Angell, 2004). Please see paper II for more detailed discussion.

It is interesting to notice that the onset temperatures of the glass transition are nearly the same for HQ and annealed hyperquenched (AHQ) samples, both of which are about 20 K higher than that for the glass formed by slow cooling. The 20 K discrepancy between the hyperquenched and normally cooled glasses leads to the question: What is the real glass transition temperature, T_g? The T_g here is quantified as the onset temperature on the DSC curves where the heat capacity of glass continuously goes up to that of the supercooled liquid (melt) state. The existence of the universal T_g of HQ and AHQ fibers implies that the backbone of the glass network relaxes only during the primary relaxation and is largely unaffected by the difference in the thermal history (annealing and quenching degree) of our samples under study. Compared to the C_p curves for slowly cooled annealed glasses, the glass transition shows the same feature, i.e., T_g is kept constant. However, DSC signals are a manifestation of complicated thermal responses and do not directly tell whether the endotherm in the glass transition range is from the glass transition or due to compensation of the recovered enthalpy. Interestingly, temperature-modulated DSC (TMDSC) measurements always give similar values of T_g for the glasses with different thermal histories (Tonchev et al, 2002, and Chen et al, 2010). In addition, the T_g value, which is obtained from the reversing heat capacity by TMDSC, is generally about 10 to 20 K higher than the value obtained by a conventional DSC. This difference is in the same range of the T_g difference between the HQ and the slow cooled samples. However, the current TMDSC cannot reach as high temperature as when using a conventional DSC. Thus, the modeling result of TMDSC for Eagle XG® (Corning commercial glass) will be presented next.

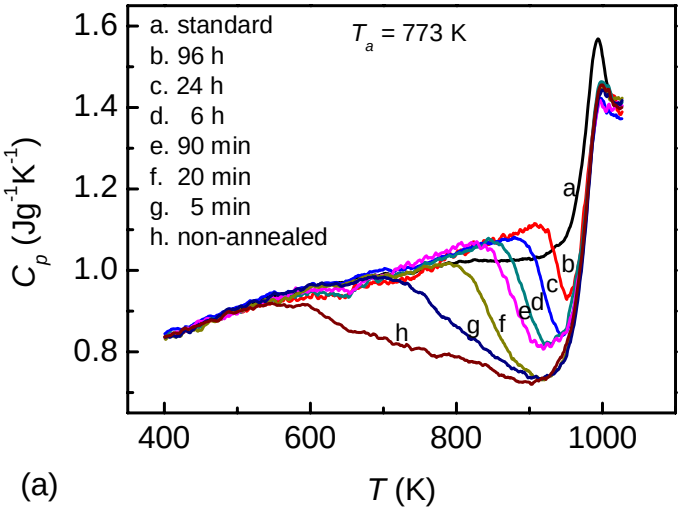
a. standard
b. 96 h
c. 24 h
d. 6 h
e. 90 min
f. 20 min
g. 5 min
h. non-annealed
T_a = 773 K
C_p (Jg^{-1}K^{-1})
T (K)
1.6
1.4
1.2
1.0
0.8
400
600
800
1000
a
b
c
d
e
f
g
h

(a)

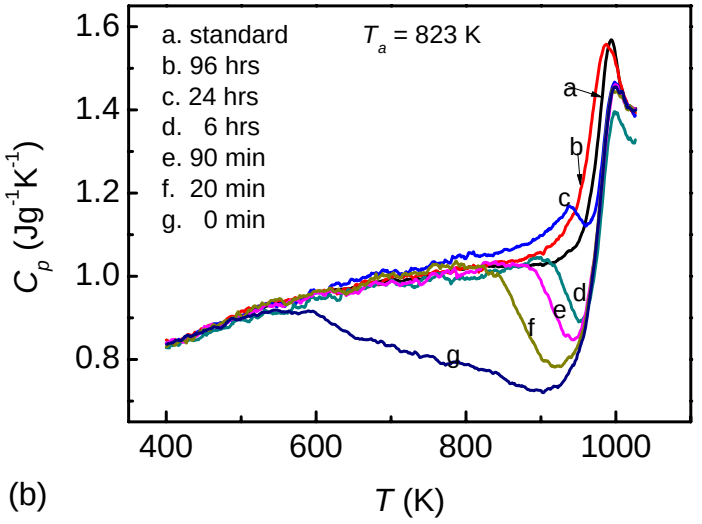
a. standard
b. 96 hrs
c. 24 hrs
d. 6 hrs
e. 90 min
f. 20 min
g. 0 min
T_a = 823 K
C_p (Jg^{-1}K^{-1})
T (K)
1.6
1.4
1.2
1.0
0.8
400
600
800
1000
a
b
c
d
e
f
g

(b)

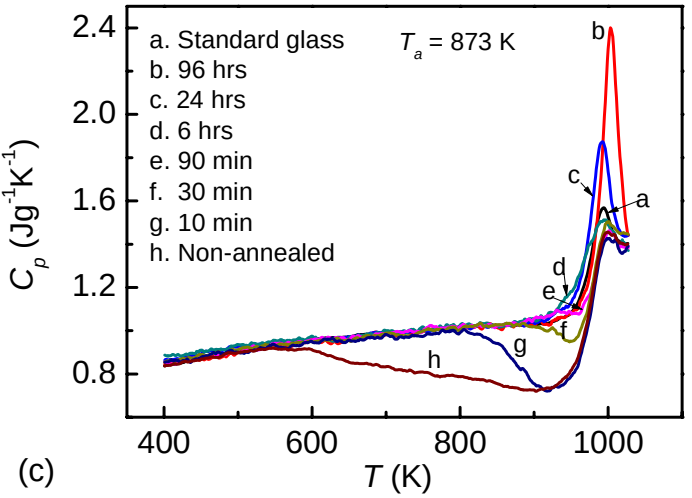

Figure 3-1. Isobaric heat capacity curves for the hyperquenched (HQ) sample, the sample cooled at 20 K/min, and the samples hyperquenched and subsequently annealed (AHQ) for various durations at the annealing temperatures (T_a): (a) 773 K; (b) 823 K; (c) 873 K.

3.2 TMDSC modeling of Glass transition

3.2.1 Heat flow deconvolution in TMDSC

The advantage of TMDSC over conventional DSC is argued as the ability to separate overlapping physical phenomena through deconvolution of the signal into reversing and non-reversing components of the total heat flow (Verdonck et al, 1999). For investigation of glassy systems, the reversing heat flow clearly shows the glass transition range while the non-reversing heat flow is a measure of structural relaxation during the TMDSC scan (Verdonck et al, 1999). In terms of glass transition study, we will focus on the reversing heat flow from TMDSC.

The output heat flow of the simulated experiment has the same feature as the modulated heat flow signal, $\dot{H}_{TMDSC}$, shown in Fig. A1(b) of Ref. (Chen et al, 2010). The average heat flow (total heat flow) and amplitude are generated by Fourier transformation. Then the total heat flow is decomposed to reversing heat flow and non-reversing heat flow for the two upscans and the downscan following the appendix of Ref. (Chen et al, 2010). In Figs. 3-2(a)-(c), the heat flows from frequency equal to 0.003 Hz is shown as an example. In all of the calculations, the solid (vibrational) heat flow has been subtracted from the total heat flow, such that only the excess (primarily configurational) heat flow is showing in all the figures.

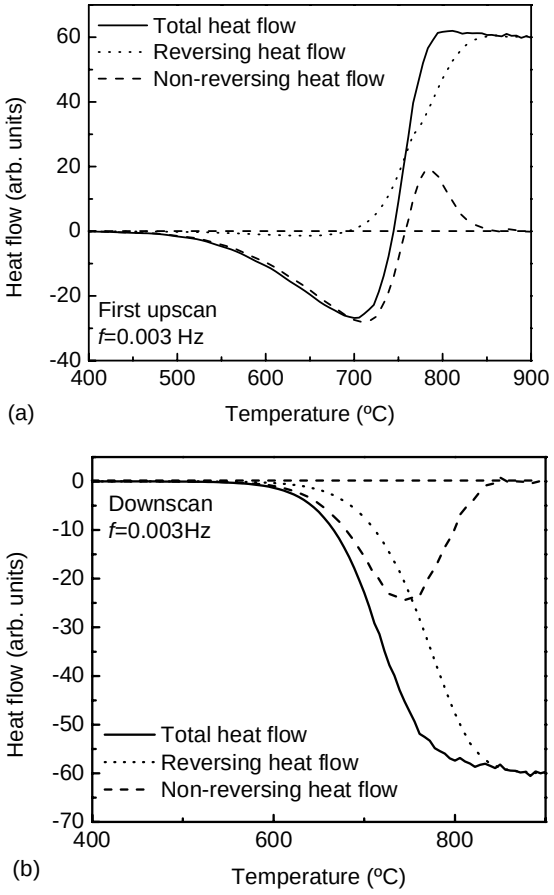

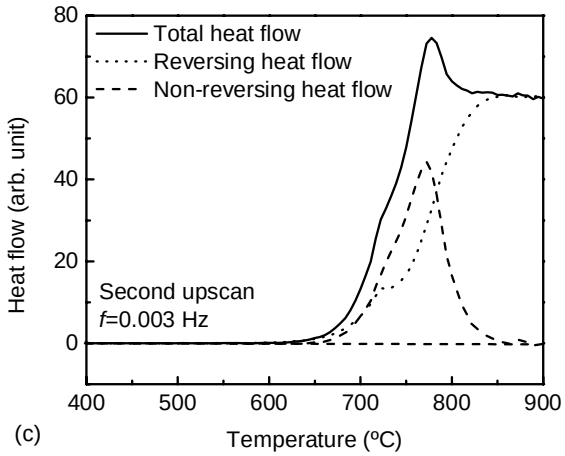

Figure 3-2. The analyzed total heat flows from the simulation. (a) first upscan; (b) downscan; (c) second upscan.

The non-reversing heat flow has attracted more attention comparing with reversing heat flow. One possible reason is that the property we can get from reversing heat flow is only the glass transition range, however, this is the right point we will focus on here. The non-reversing heat flow will be discussed in chapter 4 in more detail. It has been noticed that the frequency dependence of non-reversing heat flow and T_g determined from TMDSC has been studied experimentally (Chen et al, 2010) and also in simulated experimental scans (Simon, 2001, and Simon and McKenna, 2000).

3.2.2 Frequency correction for reversing heat flow

The frequency dependence of non-reversing heat flow results from the frequency dependence of the reversing heat flow since the non-reversing heat flow is subtracting the reversing heat flow from the total heat flow. Thus, the glass transition from reversing heat flow is also frequency dependent. However, the glass transition from TMDSC won't be comparable with that from conventional DSC. In

addition, T_g from one linear heat rate is not related to one viscosity or relaxation time. From this point of view, the T_g from TMDSC is not as meaningful as that from conventional DSC. It is expected that one identical T_g could be obtained for one linear heating rate for the TMDSC. Thus, the frequency correction will also be performed for the reversing heat flow to verify whether one unified T_g existing in TMDSC. The first case will be presented is T_g for the rejuvenated EAGLE XG® glass where the cooling rate of this rejuvenated glass is 1 °C/min. The total heat flow from TMDSC is identical to the output of conventional DSC. Thus, the T_g for the rejuvenated glass from conventional DSC (total heat flow) is about 726 °C at heating rate of 1 °C/min. Without the frequency correction, the T_g values are distributed between 764 °C and 795 °C in the frequency range from 0.002 Hz to 0.01 Hz as shown in the inset of Fig. 3-3(a). After applying the frequency correction, one common T_g is obtained as 713 °C. The temperature corresponding to 10^{12} Pa-s viscosity for EAGLE XG® glass is 735.7 °C. Following the MYEGA viscosity model and the parameters listed in Ref. [30] for EAGLE XG®, viz., $\log(\eta_\infty)$ =-3, T_g =735.7 °C, and m =32.5, the corresponding equilibrium viscosity values at the above temperatures are: $10^{12.8}$ Pa-s (at 713 °C), $10^{12.3}$ Pa-s (at 726 °C), $10^{11.1}$ Pa-s (at 764 °C), and $10^{10.3}$ Pa-s (at 795 °C).

As we expected above, one unified T_g exists from TMDSC measurement when the heating rate is identical. If we use the linear heating rate of 1 °C/min in TMDSC, T_g should be a unique value. Thus, either the value from the total heat flow or the value from the frequency corrected reversing heat flow could be selected as T_g. But since these two values have an offset of 13 °C, which value should be used as T_g? To answer this question, we must compare these values to T_g determined upon cooling from the liquid state, which should be considered as the real T_g. According to the calculation of frequency correction for reversing heat flow in heating, the frequency corrected reversing heat flow during cooling is the sum of the measured reversing heat flow and the non-reversing heat flow during cooling, which is identical to the total heat flow in cooling. Thus, T_g in cooling is determined only by the total heat flow. Finally, T_g is found

to be 713 ^{o}C when the linear cooling rate is 1 ^{o}C/min, which is exactly the value obtained from the frequency corrected reversing heat flow.

We now further check the glass transition temperature of the quenched EAGLE XG® glass. As shown in Fig. 3-3(b), T_g from reversing heat flow is also frequency dependent before the frequency correction. It shows a similar trend as with the rejuvenated glass in Fig. 3-3(a): the higher the modulation frequency, the higher the temperature at the inflection point of reversing heat flow curve. After the frequency correction, the opposite trend is observed, i.e., the reversing heat flow curve for the low frequency appears at the high temperature side. However, the reversing heat flow curves for 0.006, 0.008 and 0.01 Hz are fully overlapped. From the master curve for the reversing heat flow in Fig. 3-3(b), the inflection point is 719 ^{o}C, i.e., 6 ^{o}C higher than that of the rejuvenated glass. The frequency corrected reversing heat flow curves of both quenched glass and rejuvenated glass for 0.006, 0.008, and 0.01 Hz are presented in Fig. 3-3 (c). All six curves are almost fully overlapped, indicating that glasses with the same composition but with different pre-TMDSC thermal histories (quenched and 1 ^{o}C/min cooling) should have a similar T_g if the same heating rate is used in the TMDSC measurement.

According to topological constraint theory, the glass transition occurs when a sufficient number of constraints in the network become rigid. For oxide glasses the vitrification process is typically controlled by angular constraints in the network (Gupta and Mauro 2009, Mauro 2009c, Smedskjaer et al 2010a, Smedskjaer et al 2010b, Smedskjaer et al 2011). In DSC/TMDSC measurements, when the glass transition occurs during upscan, the network is becoming more floppy. The glass structure is influenced by the thermal history of the glass, e.g. cooling rate and annealing temperature and time. However, the very narrow range of glass transition temperatures obtained for the quenched and rejuvenated glass at the same TMDSC heating rate implies that the structure of the constraint controlling glass transition is not significantly affected by the cooling rate. This is in good agreement with our DSC study of the physical aging of hyperquenched glass fibers, where the glass transition temperatures of

hyperquenched and annealed hyperquenched glasses are found to be independent of thermal history (Guo et al, 2012).

This finding can now be directly verified through the measurement of T_g using the frequency corrected reversing heat flow in TMDSC. The heat flow in the cooling cycle is exothermic. In order to compare with the endothermic heat flow in the heating cycles, the opposite of the total heat flow in the cooling cycle of TMDSC measurement is also included in Fig. 3-3(c). This clearly shows that the opposite of the total heat flow during downscan lies on top of the frequency corrected reversing heat flow of the rejuvenated glass. Thus, T_g obtained from the frequency corrected reversing heat flow in TMDSC is close to that from the cooling cycle of conventional DSC. Concerning the specific case of T_g determination, the TMDSC approach is more complicated than the conventional DSC approach using a single cooling cycle. However, the conventional DSC may not be a good approach for determining the real T_g since the glass transition range is overlapped with simultaneous enthalpy relaxation.

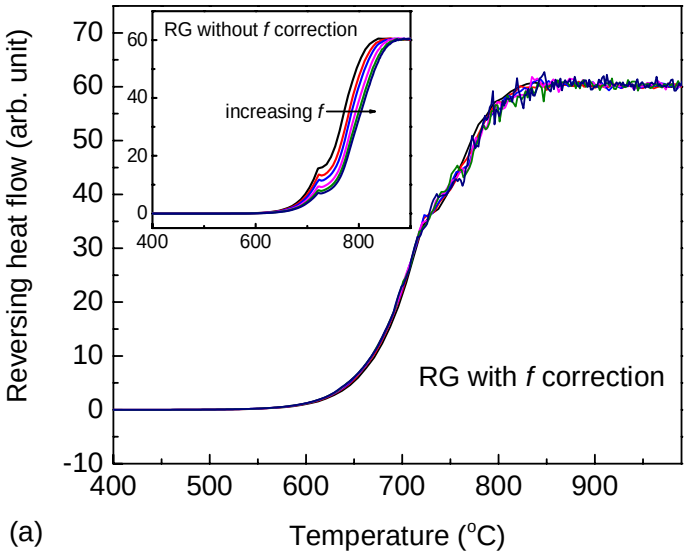

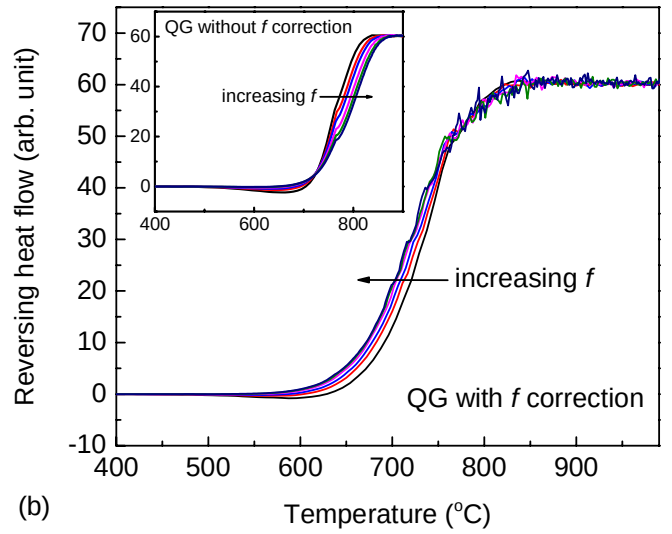

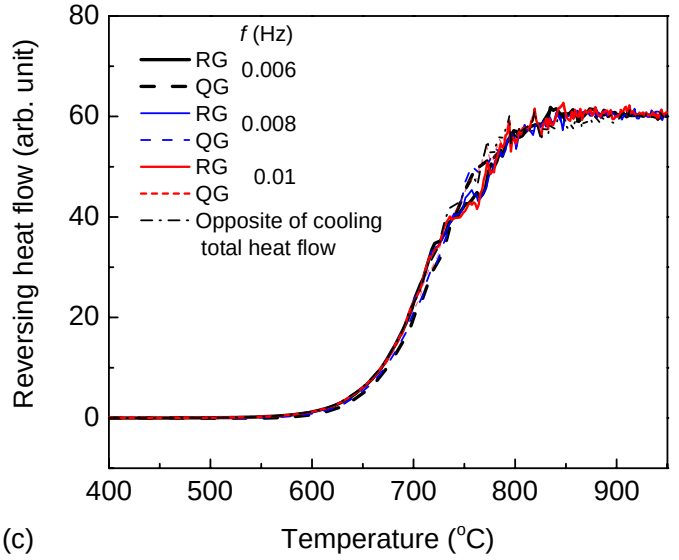

Figure 3-3. The reversing heat flow with frequency (*f*) correction: (a) rejuvenated glass (RG) showing a master curve for f = 0.002, 0.003, 0.004, 0.006, 0.008, 0.01 Hz; (b) quenched glass (QG) showing a master curve for f = 0.006, 0.008, 0.01 Hz; (c) rejuvenated glass (RG) and quenched glass (QG) for f = 0.006, 0.008, 0.01 Hz and the opposite of the total heat flow in cooling (The heat flow in cooling is exothermic, other than endothermic in heating. In order to see how

comparable with endothermic heat flow, the opposite of the total heat flow in cooling is drawn here).

3.3 Brief summary

The experimental glass transition of hyperquenched and annealed hyperquenched basaltic fibers shows that the glass transition temperature has faint thermal history or structure dependence. The simulated glass transition temperature for EAGLE XG® glass by doing frequency correction to the reversing heat flow in TMDSC also shows weak thermal history or structure dependence. These two results both prove that the constraint controlling glass transition is independent on thermal history. Finally T_g is only determined by glass composition and the heating or cooling rate in the T_g measurement.

4. **Thermodynamic Glass State**

Although the glass transition is only dependent on glass composition and heating/cooling rate in the characterization process, the glass structure is a function of the glass composition and the whole thermal history since prior cooling the equilibrium liquidus state. The thermal history is sometimes a very complicated function expressed by temperature and time. The development of fictive temperature or configurational temperature significantly simplified the problem although it is not a perfect expression for glass state or structure. Among all the fictive temperature definitions, Moynihan's fictive temperature focused on macroscopic property, which avoids unnecessary misunderstanding. Thus, our work about determining the fictive temperature of glass of arbitrary thermal history is based on Moynihan's definition. Before proceed with the unified approach for obtaining fictive temperature, we will first manifest TMDSC having advantages over conventional DSC other than the proof of glass transition range from reversing heat flow in chapter 3.

As shown in Fig. 3-2 (a)-(c), the total heat flow of quenched glass and rejuvenated glass in TMDSC measurement present different signals which reveals that the enthalpy recovery in quenched glass and rejuvenated glass have different temperature response. The reversing heat flow (after deconvolution) is designated corresponding to the glass transition whereas the non-reversing heat flow is the aging enthalpy in the TMDSC measurement process. Thus, the non-reversing heat flow in TMDSC is of great importance to represent the glass structure.

4.1 Non-reversing heat flow in TMDSC

After separating the non-reversing part from the total heat flows for different modulation frequencies, the frequency correction for the non-reversing heat flow could be obtained by adding the (negative) non-reversing heat flow during cooling to the non-reversing heat flow calculated on heating.

4.1.1 Frequency correction of non-reversing heat flow

The final non-reversing heat flows with and without the frequency correction are plotted in Figs. 4-1(a) and (b) for the quenched glass and Figs. 4-1(c) and (d) for the rejuvenated glass over the full range of modulation frequencies. The solid lines in these figures show the continuous non-reversing heat flow for each frequency >0.001 Hz, and the dotted lines shows for the results for the two lowest modulation frequencies (0.0005 and 0.001 Hz). When the modulation frequency is too low for the given linear heating/cooling rate, there are insufficient thermal cycles of the periodic perturbation within the glass transition range. This results in an effective local heating rate in the TMDSC that is significantly different from the intended linear upscan rate. Finally, as we can see the curves obtained at 0.0005 Hz and 0.001 Hz in Figs. 4-1(a) and (c), the measured heat flow will deviate from the relative higher frequencies. As shown in Figs. 4-1(b) and (d), there is a clear departure of the two lowest frequencies even after the frequency correction. For the rejuvenated glass, we obtain wholly overlapped non-reversing heat flows from 0.003 to 0.01 Hz. However, the appropriate lower bound on frequency for the overlaid non-reversing heat flow seems to have increased to 0.006 Hz for the quenched glass.

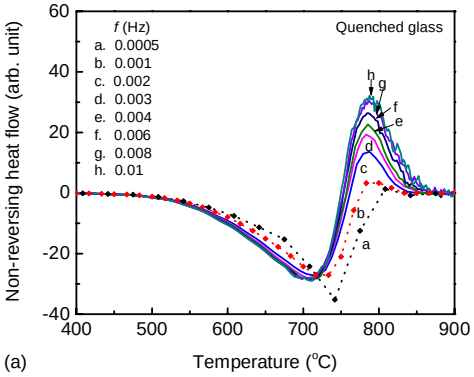
f (Hz)
a. 0.0005
b. 0.001
c. 0.002
d. 0.003
e. 0.004
f. 0.006
g. 0.008
h. 0.01
Quenched glass
Non-reversing heat flow (arb. unit)
Temperature (°C)

(a)

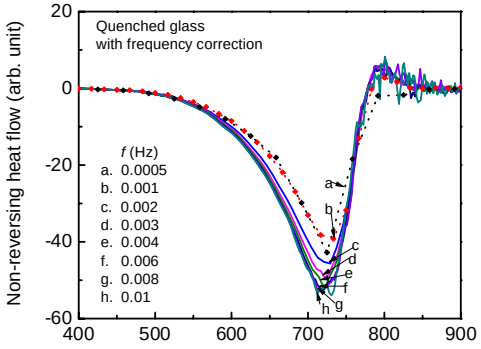
Quenched glass
with frequency correction
f (Hz)
a. 0.0005
b. 0.001
c. 0.002
d. 0.003
e. 0.004
f. 0.006
g. 0.008
h. 0.01
Non-reversing heat flow (arb. unit)
Temperature (°C)

(b)

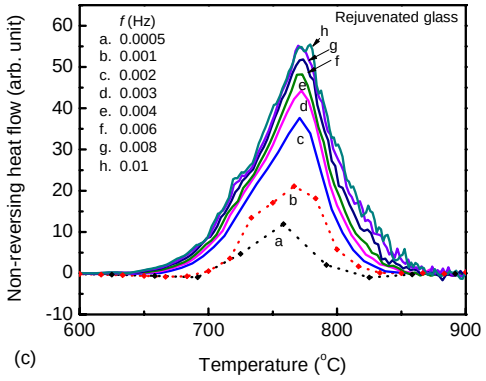
f (Hz)
a. 0.0005
b. 0.001
c. 0.002
d. 0.003
e. 0.004
f. 0.006
g. 0.008
h. 0.01
Rejuvenated glass
Non-reversing heat flow (arb. unit)
Temperature (°C)

(c)

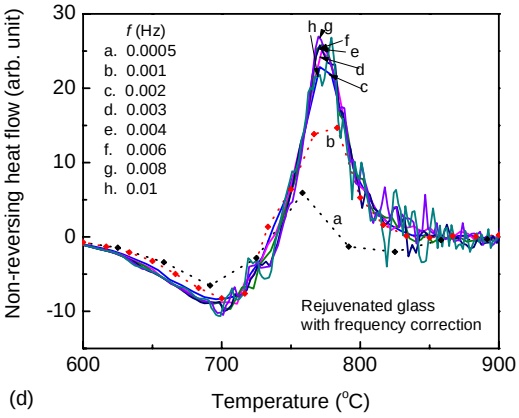

Figure 4-1. The non-reversing heat flow at modulation frequencies (*f*) from 0.0005 to 0.01 Hz: (a) quenched glass; (b) quenched glass with *f* correction; (c) rejuvenated glass; (d) rejuvenated glass with *f* correction.

4.1.2 Enthalpy recovery from non-reversing heat flow

One application of non-reversing heat flow in TMDSC is determination of the enthalpy recovery of a glass during aging, i.e., the area enclosed in frequency corrected non-reversing heat flow curves of the quenched and rejuvenated glass. This area is taken as the enthalpy difference between the quenched and rejuvenated glass during the TMDSC upscans (Chen et al 2010). The non-reversing heat flows after frequency correction of quenched and rejuvenated glasses are shown in Fig. 4-2. The total heat flows of both quenched and rejuvenated glasses are represented by the green curves in the same figure. The area enclosed by the total upscan heat flows of quenched and rejuvenated glasses is taken as the total aging enthalpy during conventional DSC measurement. In the case of TMDSC, the area enclosed by non-reversing heat flows after applying the frequency correction to the quenched and rejuvenated glasses is also taken as the total aging enthalpy. Therefore, both techniques should yield the same value for the aging enthalpy. For our simulation of EAGLE XG®, the area enclosed by the green total heat flow in Fig. 4-2 is 6114 arbitrary units, while the area enclosed by the frequency-

correction non-reversing heat flow from TMDSC is 6116 arbitrary units (here selecting 0.01 Hz as the modulation frequency). The excellent agreement between these two results indicates that non-reversing heat flow after frequency correction is a good representation of the total aging effect.

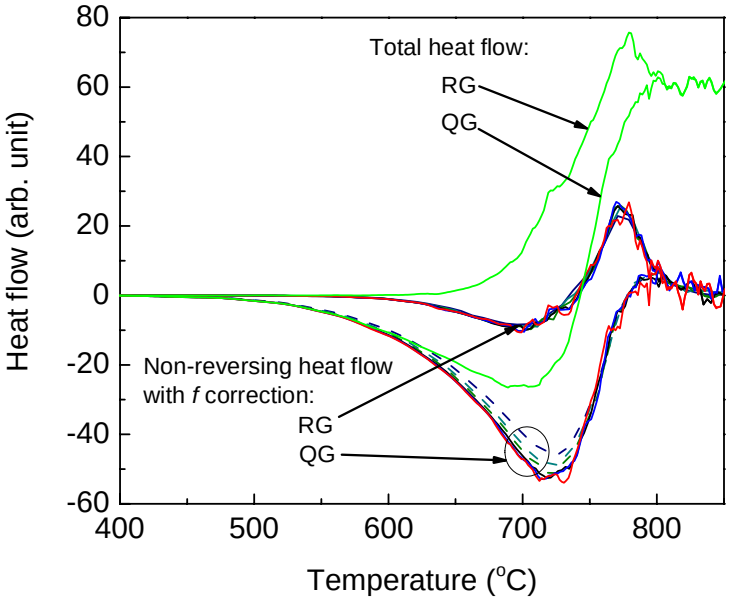

Figure 4-2. The area enclosed by the non-reversing heat flow master curves of quenched glass (QG) and rejuvenated glass (RG) for frequencies (*f*): 0.002, 0.003, 0.004, 0.006, 0.008, 0.01 Hz, comparing with the area enclosed by the total heat flow curves of QG and RG.

4.2 Thermodynamic glass state determination

4.2.1 The limitation of existing approaches

4.2.1.1 Moynihan's area matching method A calorimetric area-matching (i.e., enthalpy-matching) approach for determining the thermodynamic fictive temperature of a glass was proposed by Moynihan et al. (Moynihan et al 1976) based on differential scanning

calorimetry (DSC), in which the isobaric heat capacity (C_p) of a sample is measured at 1 atm along a linear temperature path. One single C_p upscan curve is utilized in this approach. The fictive temperature derived using this method reflects the structural contribution to the enthalpy of a glass, i.e., the temperature at which the equilibrium liquid has the same structural enthalpy as the glass sample. The Moynihan routine requires that the upscan rate of the DSC be of similar magnitude as the cooling rate of the initially formed glass, usually 10 or 20 K/min. Moynihan *et al*. (Moynihan et al, 1976) also determined the T_f of the B_2O_3 glass cooled at 80 K/min in DSC based on the area matching approach with an upscan rate of 10 K/min. Due to this mismatch of cooling and upscan rates, they observed a small exothermic peak on the C_p curve, the area of which was considered during the T_f determination procedure. However, the Moynihan routine cannot be used for rapidly cooled (hyperquenched) glasses where the cooling rate (q) is much faster than any possible scan rate in a laboratory DSC. For instance, Fig. 4-3 shows the heat capacity measured using DSC of basaltic fiber hyperquenched at 10^6 K/s. As shown in this figure, the measured heat capacity from the DSC corresponds to the glassy heat capacity only at temperatures lower than 550 K. The measured heat capacity at temperatures higher than 550 K is a mixture of the glassy heat capacity and an exothermal peak due to relaxation. The exothermal peak is so broad and intense that the extrapolation of the glassy heat capacity to high temperature cannot be determined from this single upscan. For example, both the red and blue curves shown in Fig. 4-3 may be considered as possible extrapolations of glassy heat capacity. However, the fictive temperature determined based on these two extrapolated curves would differ greatly.

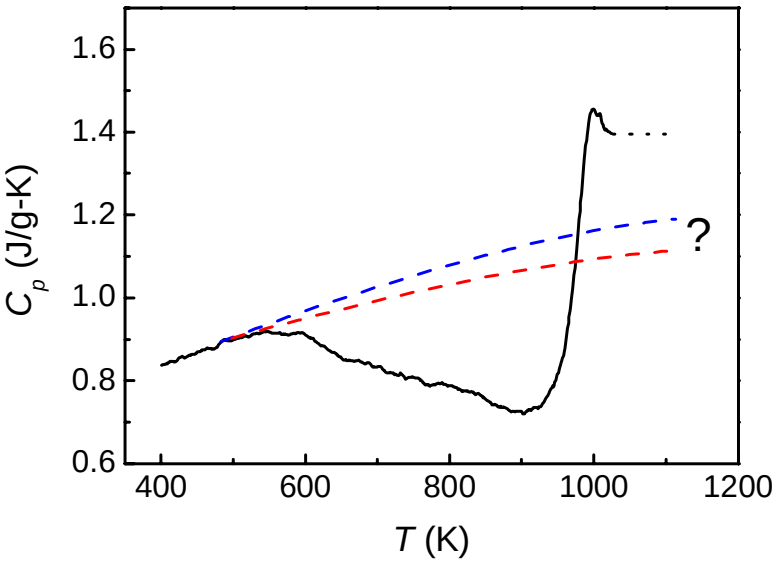

Figure 4-3. Representative measured heat capacity curve (solid line) of hyperquenched glasses where the heating rate for the DSC upscan is 20 K/min. The dashed lines and the question mark show the uncertainty of extrapolating the glass heat capacity encountered when the second standard upscan is missing.

4.2.1.2 Fictive temperature of hyperquenched glass fiber A method for determining T_f of hyperquenched ($q \approx 10^6$ K/s) glass fibers was proposed by Yue *et al*. (Yue et al, 2002a and Yue et al, 2004b) and independently by Velikov *et al*.(Velikov et al, 2001) based on two consecutive C_p curves at the same upscan rate. The first upscan yields the C_p curve of the initially formed hyperquenched (HQ) glass, $C_{p1}(T)$, where the precise quench rate may not be known. This first upscan is followed by downscan of the sample at a cooling rate equal to the heating rate of the upscan. A second upscan of the DSC is then performed on this "rejuvenated" glass using the same scan rate as previously. The integrated difference between the heat capacity of the rejuvenated glass, $C_{p2}(T)$, and the HQ glass, $C_{p1}(T)$, gives the enthalpy

difference due to the thermal history difference of the two scans, which can then be used to determine the fictive temperature of the initially formed glass. The Yue method is manifested by Eq. (4) in Ref. (Yue et al, 2002a) and theoretically can be applied for determining T_f of a glass with any thermal history. However, it should be stressed that the graphical method shown in Fig. 2 of Ref. (Yue et al, 2002a) is only applicable for the glass with a fictive temperature T_f higher than T_{eq} (the onset temperature of the liquid equilibrium), since only in this case the integration term $C_{p,liquid}$-C_{pglass} in Eq. (4) of Ref. (Yue et al, 2002a) is equal to the term (C_{p2}-C_{p1}). In the case of T_f<T_{eq} the abovementioned two terms are not interchangeable. Ref. (Yue et al, 2002a) did not graphically show how to apply its Eq. 4 in determining the T_f of the glass in the case of $T_f < T_{eq}$. It should be mentioned that the Yue method was incorrectly applied by several other scientists for the case of $T_f < T_{eq}$ (Johari and Aji 2010). In addition, the Yue *et al.* method requires that the second upscan should be made at the standard rate of 10 K/min in order to determine the standard glass transition temperature, T_g that is needed to find the T_f of a glass. It is desirable to have a general, unified approach for the calorimetric determination of fictive temperature both graphically and numerically.

4.2.2 Generalized approach

In Fig. 4-4 we present a general routine for rigorous determination of fictive temperature for glasses of any thermal history (e.g., annealed or hyperquenched) under isobaric conditions. Our method reveals a thermodynamic signature of glass that is independent of kinetic effects due to changes in DSC upscan rate (Velikov et al, 2001 and Scherer, 1992). As with the Yue *et al.* approach, (Yue et al, 2002a and Yue et al, 2004b) the technique involves comparing $C_{p1}(T)$ and $C_{p2}(T)$ from two consecutive upscans of the DSC at the same heating rate. The thermal history of the glass prior to measurement need not be known. The two upscans are interposed by a downscan. Unlike previous methods, there is no restriction on the particular value of the DSC upscan rate.

The new technique involves three area-matching steps, illustrated in Figs. 4-4 (a)-(c). The first step involves calculation of T_{f2}, the fictive temperature of the rejuvenated glass. Theoretically, the fictive temperature of any glass is independent of the heating rate during upscan, which is also proved by our experiment and the new technique as shown below. Thus, the heating rate for the second upscan does not need to be the same to previous cooling rate. However, in order to make the problem simple, the upscan rate is set to be equal to the previous downscan rate in the development of the routine. The value of T_{f2} must satisfy the area-matching condition of Fig. 4-4(a) to ensure that the structural enthalpy of the glass is equal to that of the equilibrium liquid at the fictive temperature. This step is similar to that proposed previously by Moynihan *et al* (Moynihan et al 1976). The second step is to calculate the enthalpy difference between the initially formed and rejuvenated glass, as depicted in Fig. 4-4 (b). This step is identical to that proposed previously by Yue *et al* (Yue et al, 2002a and Yue et al, 2004b). The final step of the calculation, shown in Fig. 4-4(c), involves calculating the fictive temperature of the initially formed glass, T_{f1}, by:

$$\int_{T_{f2}}^{T_{f1}} \left(C_{\text{p liquid}} - C_{\text{p glass}}\right) dT = \int_{0}^{\infty} \left(C_{p2} - C_{p1}\right) dT \,. \qquad (4\text{-}1)$$

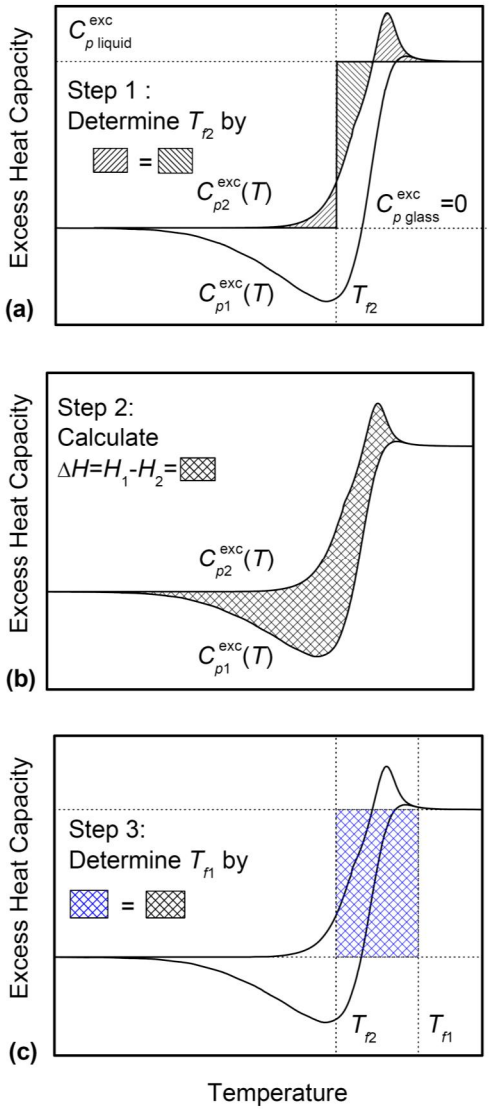

Figure 4-4. Graphical representation of the three-step procedure for determining the calorimetric fictive temperatures T_{f1} and T_{f2}. (a) First, calculate the fictive temperature of the rejuvenated glass, T_{f2}, on the second upscan using the illustrated area-matching. (b) Second, calculate the area between the two DSC upscan curves, which gives the difference between the enthalpies of as-formed(H_1) and rejuvenated glasses(H_2). (c) Finally,

determine the fictive temperature of the as-formed glass, T_{f1}, by area-matching using Eq. (4-1).

The unified approach was tested and found valid for the annealed soda lime silicate glass as described in Paper 1. And a glass scanned by 4 different heating rates was calculated to have identical fictive temperature, which proves that the area-matching routine successfully isolates the thermodynamic value of T_{f1} independent of the kinetic factors during measurement.

4.2.3 Numerical validation of the unified approach

Considering the heating rate limitation in DSC measurement, a thorough validation of the area-matching technique was performed using a series of simulated DSC "virtual experiments" for a model glass. The modeling setup has been described in Chapter 2. The simulated glasses are formed by linearly cooling an initially equilibrated liquid from 1498 to 298 K. The initial cooling rates (q) are between 10^{-3} and 10^{6} K/s to cover the full range of realistic thermal histories from very slowly annealed to hyperquenched. The initially cooled glasses are then subjected to two DSC upscans between 298 and 1498 K, with an intervening downscan at the same rate. The DSC scan rates are varied from 10^{-3} to 10^{3} K/s, well beyond the realistic limits of a laboratory DSC. The high final temperature is chosen to ensure equilibration of the liquid for even the fastest simulated DSC scans considered.

Figure 4-5 (a) compares the derived values of T_{f1} using the area-matching method versus the known as-formed values of T_{f1} given by the model. Here we show results using a stretching exponent of $\beta = {}^{3}/_{5}$, the characteristic value for short-range forces (Phillips, 1996). The standard deviation of error between the derived and actual fictive temperature is 0.046 K. We found similarly excellent agreement for all other values of β. The results in Fig. 4-5 (a) confirm that the area-matching method of Fig. 4-4 is applicable for all thermal histories and yields T_{f1} values that are independent of DSC scan rate, effectively

separating the thermodynamic signature of the glass from the kinetic aspects of DSC measurement. The impact of cooling rate on fictive temperature, as elucidated by Moynihan (Moynihan et al, 1974, and Moynihan et al, 1976), can be seen in the values of T_{f2} for the second upscan, plotted in Fig. 4-5 (b).

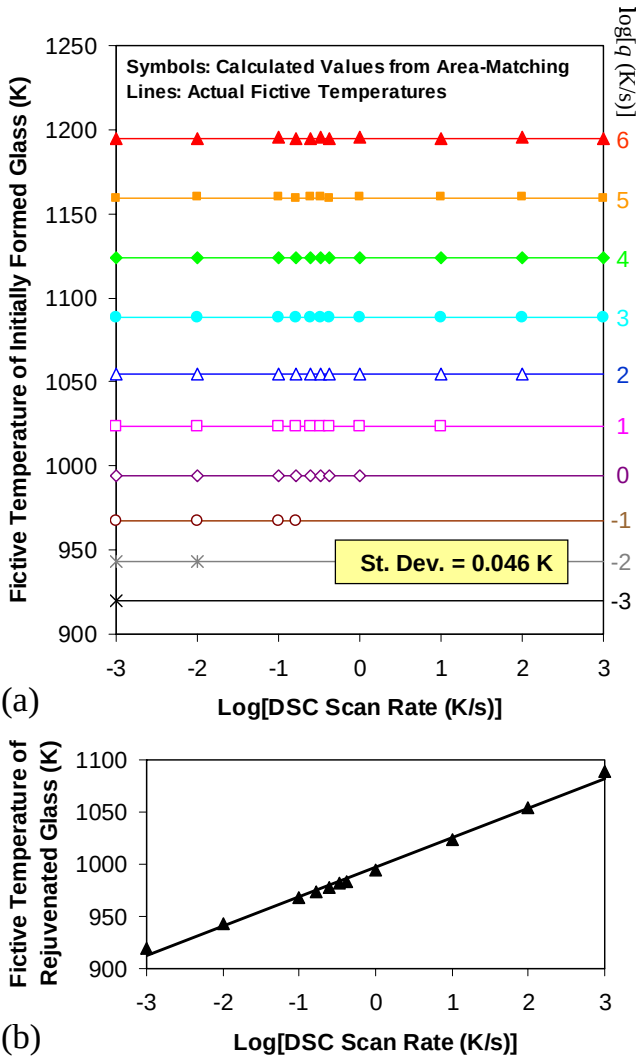

Figure 4-5. (a) Results of T_{f1} calculations using the simulated DSC with initial cooling rates between 10^{-3} and 10^{6} K/s and scan rates between 10^{-3} and 10^{3} K/s. The derived values of T_{f1} using area-matching (symbols)

are in excellent agreement with the actual fictive temperatures from the relaxation model (lines). The missing points in the lower-right corner of the figure are due to computational limitations using the Mazurin-Startsev algorithm, which produced near-vanishing time steps in these particular cases. (b) The kinetic effect of cooling rate on the glass transition is evident in the value of T_{f2}, which varies linearly with the logarithm of DSC scan rate, as expected from the work of Moynihan *et al* (Moynihan 1976)

4.2.4 Advantage of the unified approach

The Moynihan technique, Yue technique, and the generalized method are all based on Moynihan's macroscopic definition of fictive temperature. Thus, for one heat capacity curve, if the same extrapolated glassy heat capacity and the liquid heat capacity are used, it could be expected that the fictive temperature from these three techniques should be the same. Furthermore, Eq. (4) in Ref. (Yue 2002a) for the Yue technique is identical to Eq. (1) in this paper if $T_{f2}=T_g$. Thus, we can say that the Yue technique is a special case of the approach proposed in this thesis. However, the graphical technique shown in Fig. 2 of Ref. (Yue 2002a) is only valid when $T_f > T_{eq}$. For the glasses whose fictive temperature is lower than T_{eq}, according to Eq. (4) in Ref. (Yue 2002a), the graphical method should be different from the one used in Fig. 2 which has been specified in the Appendix of paper 1.

In comparison with the previous approaches, the present generalized one addresses the following crucial aspects:

First, the present approach incorporates both the Moynihan and the Yue methods. In addition, it uses any reference temperature T_{f2} for determining the T_{f1} of glasses with any thermal histories. Although in principle the Yue approach (i.e., Eq. (4) in Ref. (Yue 2002a)) can be used to determine the fictive temperature of the glasses with $T_g<T_f<T_{eq}$, e.g., the graphical method has not been specified in Ref. (Yue 2002a).

Second, it is experimentally proved that the fictive temperature of a glass calculated with this method does not depend on the upscan

rate in DSC. In addition, neither the first downscan rate nor the second upscan rate will influence the derived fictive temperature of the interested glass. Furthermore, the second upscan rate does not need to be the same as the first downscan rate.

Third, using numerical simulations where the exact fictive temperature of the glass is known, we have shown that the calorimetric area-matching technique reproduces the known fictive temperature with excellent accuracy, independent of the upscan rate used during measurement.

Finally, we emphasize a fundamental difference between the often confused quantities of fictive temperature (T_f) and glass transition temperature (T_g). The latter is an inherently *kinetic* property, defined as the temperature at which the glass-forming system has a structural relaxation time equal to an external observation time scale (Moynihan et al 1976, and Mauro et al, 2007) (typically taken as 100 s for molecular glasses, and 30-40 s for oxide glasses, or at a fixed shear viscosity of 10^{12} Pa-s). The fictive temperature, in contrast, is an inherently *thermodynamic* property. Our technique illustrated in Fig. 4-4 enables this thermodynamic order parameter to be determined independently of the kinetic effects during measurements. Such decoupling of thermodynamics and kinetics is necessary for building a complete and coherent understanding of the glassy state.

As discussed in this paper, the excess C_p can be regarded as a constant for most oxide glasses since the liquid C_p is nearly constant and the extrapolated glass C_p is close to a constant above the glass transition. However, organic glass formers like polymer systems could show an increase or a decrease of the liquid heat capacity with temperature, depending on the nature of the systems. Therefore, more attention should be paid to the calculation of excess heat capacity when considering different glass systems.

The general routine was only tested under ambient pressure. It is expected that the method could be applicable to the glasses under

other pressures. However, the technique is not applicable under varying pressures (i.e., non-isobaric conditions), where a fictive pressure may also be considered. The determination of T_f values of the glass as a function of the pressure has been discussed elsewhere (Yue et al, 2007 and Wondraczek et al, 2007a and 2007b).

4.3 Brief summary

The thermodynamic state of a glass is measurable for specific physical properties such as volume, density and enthalpy and so on. According to Moynihan's fictive temperature definition, fictive temperature could be a scale for description of the glass state. DSC has been used as a well-known technique to determine the enthalpy state of a glass. In this chapter, we first clarify that the frequency correction is necessary for generating useful information from non-reversing heat flow in TMDSC. Then, a unified approach for determining the enthalpic fictive temperature of a glass formed by an arbitrary cooling is proposed which follows Mohnihan's definition but unifies the graphical aspects of Moynihan's and Yue's techniques. The calorimetric area-matching technique has been proven that reproduces the known fictive temperature with excellent accuracy, independent of the upscan rate used during measurement. Using our technique we accurately determined the fictive temperatures of glasses where the complicated endotherm and exotherm peaks shown in the C_p curves, for instance, (1) highly annealed glasses; (2) drawn glasses (Ellison and Cornejo, 2010) and (3) annealed hyperquenched glasses.

5. Structural relaxation in annealed hyperquenched basaltic glasses

From the beginning of this thesis, we have talked about experimental and modeled glass transition and glass state. In this chapter, we will present another very important yet not well understood topic, viz., glass structural relaxation, which occurs in all glass systems. In the case of glass transition during cooling and heating, glass transition is accompanied by the structural relaxation rate of liquid and glass. Several phenomenological models have been developed for describing the structural relaxation of liquid as discussed in 2.1. The difficulty of structural relaxation of glasses, which are out of equilibrium, has been explained in the introduction part of this thesis. Besides the nonequilibrium viscosity measurement by beam bending viscometer, the relaxation of glasses has also been studied by enthalpy recovery in a heat treatment process. Systematic study of the enthalpy recovery of hyperquenched basaltic fibers during post forming heat treatment is performed to gain more knowledge of structural relaxation.

The enthalpy recovery of the hyperquenched basaltic fiber in the post forming heat treatment process obeys the KWW function as described in the 2.3. Thus the enthalpy recovery can be calculated by

$$H(T_f(t)) - H(T_{f,final}) = (H(T_{f,0}) - H(T_{f,final})) \cdot \exp(-(t/\tau)^{\beta}) \quad (5\text{-}1)$$

where $H(T_{f,0})$ is the enthalpy of the as-hyperquenched glass with the initial fictive temperature $T_{f,0}$, $H(T_{f,final})$ is that of the fully relaxed (i.e., long-time annealed) HQ glass with the final fictive temperature $T_{f,final}$, and $H(T_f(t))$ is that of the HQ glass with a fictive temperature at any time, t, during the annealing process.

5.1 Specific heat measured by DSC

The as-formed basalt fibers were subjected annealing at temperature from 573 K to 873 K for different dwelling times. The

specific heat of the as-formed hyperquenched basaltic fibers and the fibers after post-forming heat treatment were measured using a differential scanning calorimeter (DSC) (Netszch Jupiter STA 449C). The detailed experiments were described in Paper 2. Two upscans with one downscan in between were carried out for each sample. The heating/cooling rate is selected as 20 K/min. Thus, the samples subjected to the second upscan were generated by slow cooling. The specific heat obtained in the second upscan is shown in Fig. 5-1(a) and the fictive temperature calculated by Moynihan's area matching method (Moynihan et al 1976). The specific heat of a fresh basaltic fiber is shown in Fig 5-1(b) and the fictive temperature is calculated by Yue's approach (Yue et al, 2002a).

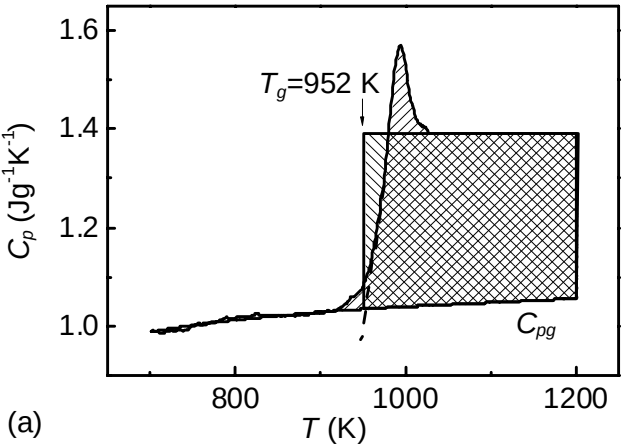

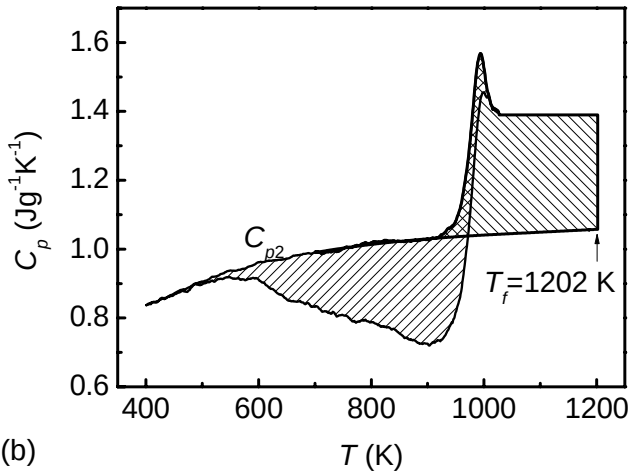

Figure 5-1. (a) Determination of T_g for the standard sample that was reheated to above the glass transition and subsequently cooled at 20 K/min. (b) Determining T_f of the hyperquenched (HQ) (as-produced) sample, where C_{p2} is the isobaric heat capacity for the sample cooled at 20 K/min. The uncertainty of T_f determined by DSC measurement is about 1%.

We annealed the basalt fibers at 473 K, however, the heat capacity curve of the four-day-annealed sample did not show an observable difference compared to the as-formed one. Thus, the annealing temperature was then increased to 573 K. From the heat capacity curves of the HQ basalt fiber annealed at 573 K (0.6 T_g) as shown in Fig. 5-2(a), we can observe that the enthalpy recovery begins when the annealing temperature is even lower than 0.6 T_g. It is reasonable if we consider that the exotherm peak for the fresh fiber begins at about 535 K where the total heat capacity of fresh fiber deviates from the vibrational heat capacity. The measured heat capacity curves of the samples annealed at 773 K (about 0.81 T_g) are shown in Fig. 5-2 (b). Comparing the enthalpy recovery for samples annealed at 573 K and 773 K, it is obvious that the enthalpy recovered during 30 days at 573 K is less than that during 20 minutes at 773 K, which means the relaxation rate is about two orders of magnitude faster for 773 K vs 573 K. A clear pre-endotherm peak appears at temperatures below T_g for samples annealed at 773 K while not observed for 573 K annealing. A

similar pre-endotherm effect has also been observed in HQ metallic glasses (Hu and Yue 2009), molecules (Wang et al 2007), and other oxide glasses (Yue et al 2002b, and Yue and Angell 2004). As suggested elsewhere (Yue et al 2002b, Inoue 1985, and Angell 2003), the pre-endotherm indicates that one structural domain relaxes faster than the others, i.e., structural and dynamical heterogeneities exist in the HQ glass (Vargheese et al 2010). While the non-existence of the pre-endotherm peak in 573 K annealed glass reveal that a lower temperature boundary is required for initiate the relaxation of the structural heterogeneous domain.

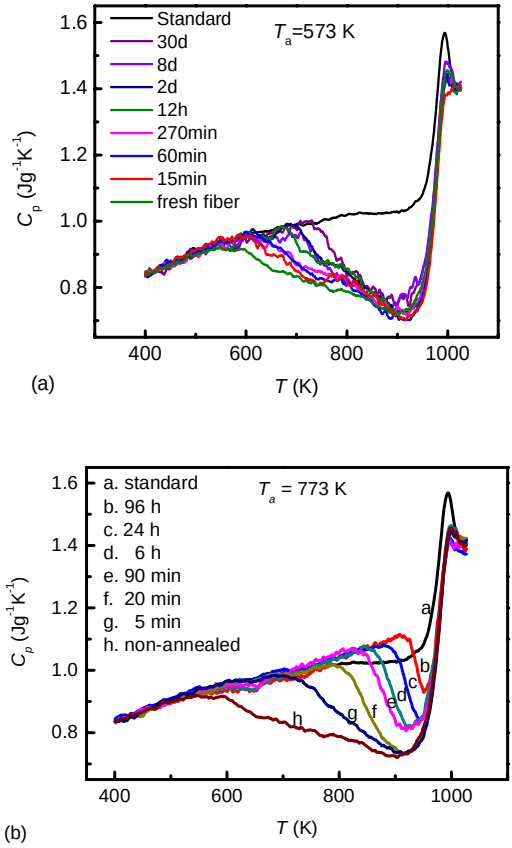

Figure 5-2. Isobaric heat capacity curves for the hyperquenched (HQ) sample, the sample cooled at 20 K/min, and the samples hyperquenched and subsequently annealed (AHQ) for various durations at the annealing temperatures (T_a): (a) 573 K; (b) 773 K.

5.2 Enthalpy recovery analysis

5.2.1 Isolation of secondary relaxation from primary relaxation

In order to visualize the annealing effect more clearly, the heat capacity difference (ΔC_p) between the AHQ and the non-annealed HQ samples is plotted in Figs. 5-3(a) and (b) taking 773 K and 873 K annealing as examples. The enthalpy difference shows the enthalpy recovery distribution clearly from annealing for different dwelling times. The low temperature portions of the enthalpy peaks for the samples annealed for different times are largely overlapped for a given annealing temperature. However, the peak of the enthalpy recovery curves rises and shifts to higher temperature with longer annealing time. Two exceptions are the samples annealed for 24 and 96 hours at 873 K, which show qualitatively different features as shown in Fig. 5-3(b). After annealing for 6 hours at 873 K, the T_f of the samples decreases down to 935 K (about 17 K lower than the T_f of the rejuvenated glass). When the annealing time is even longer, the enthalpy recovery is manifested by two exothermic peaks. For lower annealing temperatures and/or shorter time, the enthalpy recovery is mainly manifested in one peak at sub-T_g temperatures. Since the primary relaxation is about 6 to 7 orders of magnitude slower than the secondary relaxation at low temperatures (e.g. at temperatures slightly above T_g) (Ngai and Paluch, 2004), the enthalpy recovery should mainly originate from secondary (β) relaxation. The secondary relaxation is found to be decoupled from primary relaxation when the fictive temperature is greater than T_g. In other words, the hyperqenching process and post forming annealing has a rather limited effect on the structural components that relax only during the primary relaxation for fictive temperature greater than T_g. When the annealing time is sufficiently long, i.e., the glass structure becomes similar to the structure of a glass cooled at 20 K/min, and the primary (α) relaxation begins to contribute to the enthalpy recovery.

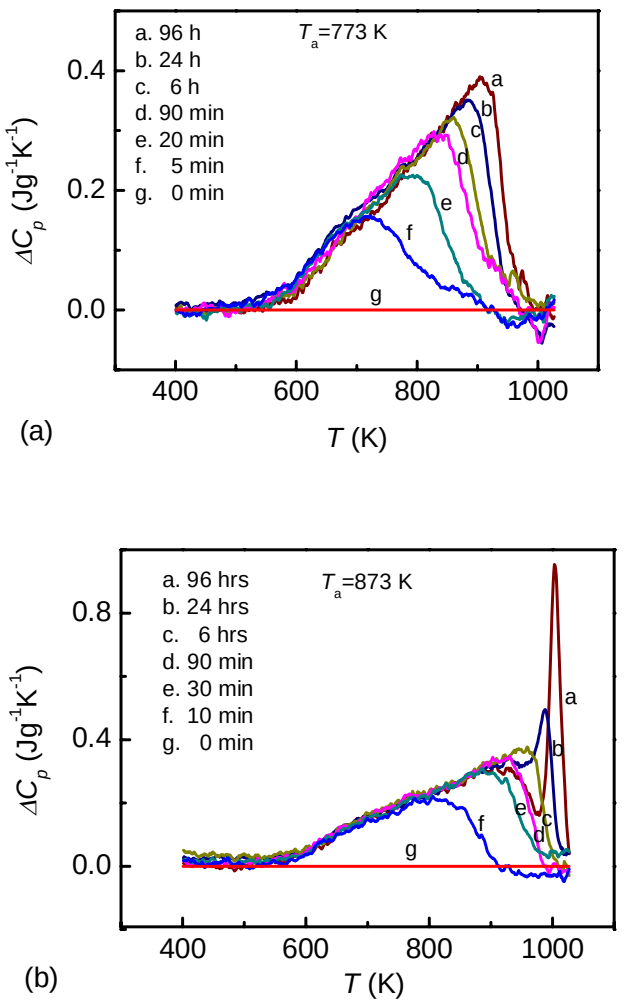

Figure 5-3. Heat capacity difference (ΔC_p) between the AHQ and the non-annealed HQ samples. The AHQ samples were annealed for various durations at the annealing temperatures (T_a): (a) 773 K; (b) 873 K.

5.2.2 Enthalpy relaxation time and stretching exponent

Normally, the equilibrium liquid state will be the final state of structural relaxation. However, the annealing temperatures are distributed from 573 K to 873 K, with a very long time required to equilibrate the samples at each temperature. At the same time, we cannot find any equation to do the extrapolation of heat capacity to temperatures far below T_g. But a reference state is indeed needed to quantify the enthalpy relaxation behavior of the HQ and AHQ samples according to equation (5-1).

As we see from the DSC curves shown in Fig. 3 of paper 2, the fictive temperatures of the HQ samples annealed for 6 h at 873 K have been reduced to values lower than T_g. As stated above and also shown in Fig. 5-3(b), for annealing times shorter than 6 h the enthalpy recovery is apparently governed by one common mechanism, i.e., secondary relaxation. However, a second mechanism (primary relaxation) may become activated at longer annealing times, e.g., 24 and 96 h at 873 K. We have excluded the data points for t = 24 and 96 h in our quantitative model of enthalpy relaxation, since two data points are not sufficient for revealing the full effect of primary relaxation on enthalpy recovery. Instead, we focus our attention on the enthalpy recovery in which the secondary relaxation is dominant, i.e., for the annealing times shorter than 6 h at 873 K and for all annealing times at the lower temperatures. The samples annealed at 873 K for 6 h have T_f of about 935 K, which is 17 K lower than the value of T_g. The T_f (i.e., 20 K lower than T_g) of the HQ samples annealed for 6 h at 873 K is chosen as the final state resulting from secondary relaxation. The samples annealed at 873 K for 24 h have a fictive temperature that is about 8 K lower than the one annealed at 873 K for 6 h. Based on the above discussion, the quantitative enthalpy recovery analysis of HQ and AHQ samples is carried out in the following way: (1) only the secondary relaxation is considered for the glasses with $T_f > T_g$-20 K at any annealing temperatures and durations; and (2) the activation energy for the secondary relaxation is a constant with respect to the glass structure.

In order to determine the stretching exponent β and the characteristic relaxation time τ, Eq. (5-1) is transformed into the expression:

$$\ln\left(\ln\left(\frac{\Delta H_{total}}{\Delta H_{remain}}\right)\right) = \beta \ln t - \beta \ln \tau \,, \qquad (5\text{-}2)$$

where ΔH_{remain} is the difference between ΔH_{total} and the enthalpy released from HQ samples during annealing, and the latter is found by calculating the area of the ΔC_p peaks in Figs. 5-3(a) and (b). We perform linear regression for the experimental ln$t$ dependence of $\ln(\ln(\Delta H_{total}/\Delta H_{remain}))$ for each annealing temperature, with β as the slope and $-\beta\ln\tau$ as the intercept, as shown in Fig. 5-4(a). The regressed values for $\ln\tau$ as a function of the inverse annealing temperatures are drawn in Fig. 5-4(b). The nearly linear relation between $\ln\tau$ and $1/T_a$ covers a T_f range of about 250 K, viz., from 1200 to 950 K. The activation energy (E) for the secondary relaxation is found to be $25.5RT_g$ (= 212 kJ/mol) independent of the fictive temperature/thermal history. The relation $E = 25.5RT_g$ is in agreement with the general empirical relation between T_g and the activation energy for the slow secondary relaxation (Kudlik et al, 1998, and Ngai and Capaccioli, 2004b). Such relation has also been found in GeO_2 (Hu and Yue, 2008) and metallic glass (Hu and Yue, 2009). The stretching exponent β is also obtained through the above regression. The stretching exponent, β, shows a strong dependence on the inverse annealing temperature, as shown in Fig. 5-4(c). This effect has also been observed in annealed metallic glasses (Hu and Yue 2009) and in the systems where relaxation shows similar stretching exponent feature to that of the relaxation of the localized state distribution in doped amorphous silicon (Kakalios et al, 1987). Fig. 5-4(c) shows that the stretching exponent follows a nearly linear relation with the inverse annealing temperatures from 623 K (0.65 T_g) to 823 K (0.86 T_g). The stretching exponent is about 0.3 when extrapolating from the low temperatures to T_g, which agrees well with non-exponential parameter of the secondary relaxation obtained from the dielectric study of molecular glass forming liquids (Wang and Richert, 2007, Wang and Sun, 2010). However, when the annealing

temperature is 873 K (0.92 T_g), the stretched exponential is greater than the linear extrapolation value from the low temperatures as shown in Fig. 5-4(c). According to Macdonald and Phillips (Macdonald and Phillips, 2005, and Phillips 1996 & 2006) and Potuzak *et al.*(Potuzak et al. 2011), the stretching exponent for structural relaxation of microscopically homogeneous glasses is 3/7 ≈ 0.43. It is obvious that the stretching exponent of relaxation time from enthalpy recovery of HQ and AHQ glass is much lower than the stretching exponent of the homogeneous glass in the previous studies (Macdonald and Phillips, 2005, and Phillips 1996 & 2006). The lower stretching exponents reported here result from the wider distribution of relaxation times in these glasses due to the presence of structural heterogeneities. The main feature of the HQ glass is the extremely fast cooling rate when the glass is made. According to the MAP model (Mauro et al, 2007b), if the fictive temperature is described as a Prony series of fictive temperature components, the fictive temperature distribution will become wider for faster cooling. If one fictive temperature component in the Prony series corresponds to single activation energy for Arrhenius type relaxation, then the activation energy distribution also becomes wider for faster cooling. In this paper, we are reporting an average stretching exponent for HQ and AHQ basalt glass. Thus, the enthalpy recovery distribution of HQ and AHQ basaltic samples is much wider than that of glass made by normal cooling, indicating a greater degree of structural heterogeneity due to the hyperquenching process. As enthalpy is recovered during annealing, the fictive temperature distribution becomes narrower until the glass is fully equilibrated at the annealing temperature, i.e., when the fictive temperature becomes equal to the annealing temperature. Therefore, the stretching exponent increases during the annealing process. While the stretching exponent during annealing at any temperature increases with time, the rate of change in the stretching exponent depends strongly on the annealing temperature itself, since the relaxation time decreases exponentially with increasing annealing temperature. Thus, the stretching exponent exhibits the relationship with inverse annealing temperatures as shown in Fig. 5-4(c).

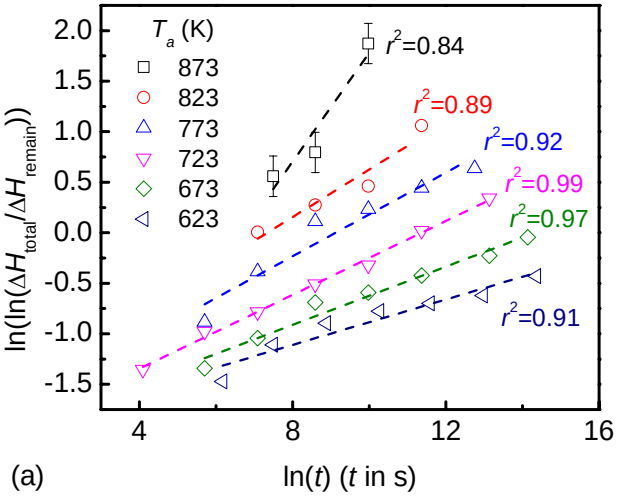
T_a (K)
873
823
773
723
673
623
r^2=0.84
r^2=0.89
r^2=0.92
r^2=0.99
r^2=0.97
r^2=0.91
ln(ln($\Delta H_{total}/\Delta H_{remain}$))
ln(t) (t in s)
(a)

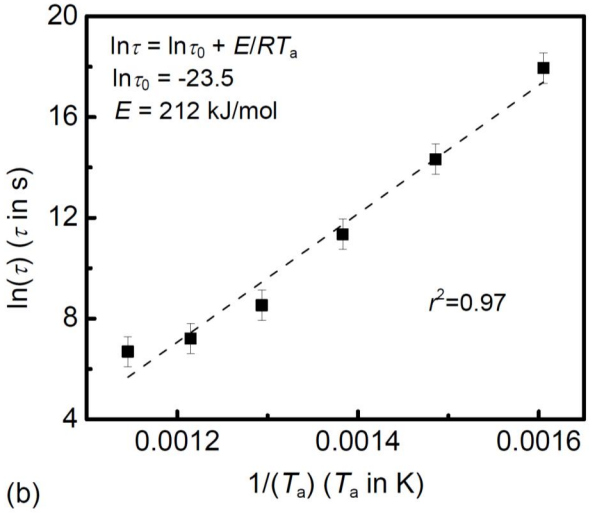
lnτ = lnτ_0 + E/RT_a
lnτ_0 = -23.5
E = 212 kJ/mol
r^2=0.97
ln(τ) (τ in s)
1/(T_a) (T_a in K)
(b)

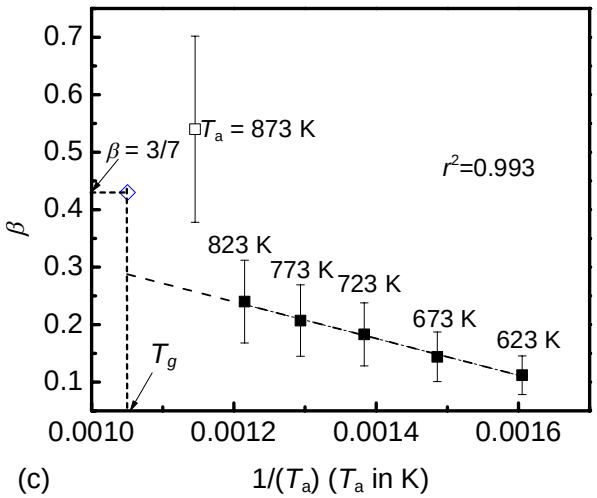

Figure 5-4. (a) The annealing time (t) dependence of the enthalpy recovery, expressed by the $\ln(\ln(\Delta H_{total}/\Delta H_{remain}))$~ln$t$ relation, where ΔH_{total} and ΔH_{remain} are the excess enthalpy in the HQ samples before and after annealing over that of the reference sample, whose T_f is 20 K lower than Tg. The HQ samples were annealed for various durations at T_a = 623, 673, 723, 773, 823 and 873 K, respectively; (b) The regressed values for $\ln\tau$ (relaxation time) as a function of inverse annealing temperatures $1/T_a$, τ_0 and E is the secondary relaxation time at the high annealing temperature limit and the activation energy, respectively; (c) The regressed values for the stretching exponent β versus the inverse annealing temperatures.

5.3 Brief summary

The enthalpy relaxation of both HQ and AHQ glasses annealing occurs mainly due to the secondary relaxation. For the high fictive temperature range from T_g-20 K to 1200 K, the secondary relaxation is fully decoupled from primary relaxation. When the fictive temperature is close to T_g, the enthalpy recovery is affected by both secondary relaxation and primary relaxation. A single fictive temperature is not sufficient in the analysis of enthalpy recovery in

HQ and AHQ basaltic samples, i.e., a distribution of fictive temperatures is required to capture the broad distribution of relaxation times. The broad distribution of activation energies for enthalpy relaxation of HQ and AHQ glasses originates from the high extent of structural heterogeneity in HQ and AHQ glasses where the structural heterogeneity is a direct result of cooling rate. Quantitatively, the stretching exponent varies with the fictive temperature distribution.

6. Heat capacity modeling from composite relaxation function

The TN model has been very successful in modeling the heat capacity curves of slow cooled and post-annealed glass. However, as shown in figure 6-1 (a) and (b), the discrepancy of modeled heat capacity curve of hyperquenched basalt fiber sample vs the experiment are : 1) the relaxation onset temperature of glasses far from equilibrium cannot be captured by TN model; 2) the enthalpy recovery is wider distributed than a stretched exponent expression; 3) the distribution at temperature close to T_g is faster than a normal stretched exponent expression.

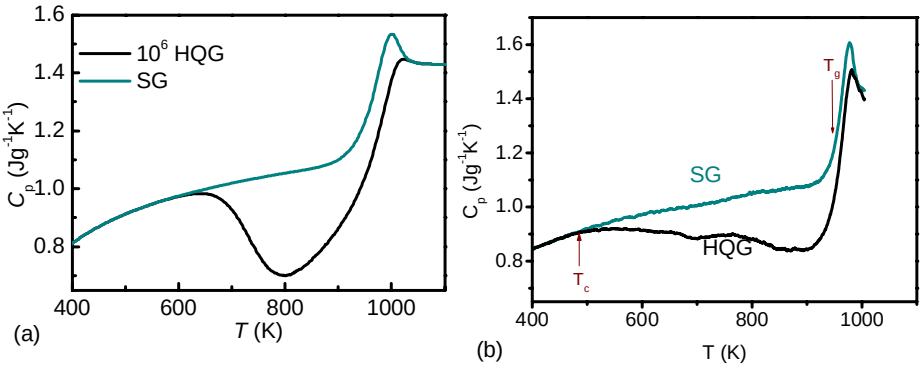

Figure 6-1. Heat capacity curves of standard cooled glass and hyperquenched glass (a) Simulated by TN model; (b) Measured in experiment.

6.1 A composite relaxation function

The heat capacity curves shown in Fig. 6-1(a) and (b) reveal that one single stretching exponent is not sufficient in simulating the whole heat capacity curve even for the fresh basalt fiber. This results strongly support the composite relaxation function model where the stretching exponent was proposed to be a product of a stretching exponent and a simple exponent as in ref. (Hornboell et al, 2010),

$$M(\xi) = \exp(-\xi^{\beta_c} - \xi) \quad (6\text{-}1)$$

where β_c is stretching exponent with a value between 0 and 1, ξ is the reduced time expressed by $\xi = t/\tau$, where t is the observation time and τ is the relaxation time. The main feature of this composite relaxation function (CRF) is that it represents a combination of two different distributions with adjusting the weight of the two terms at different relaxation rate: 1) In one case when reduced time is a large value (the relaxation time is short), the single exponent term will govern the whole CRF function. This corresponds to the fast and narrow heat capacity jump at temperatures around T_g. 2) On the other hand, when the reduced time is a small value, the stretching exponent term will control the whole CRF function. This is well related to the slow and wide distribution of the exotherm peak in the heat capacity curve.

However, the combination of a stretching exponent and a single exponent cannot give a dramatic low onset temperature for the exotherm peak. The simulated heat capacity curve for hyperquenched basalt fiber utilizing combination of a constant stretching exponent (0.2, 0.4 and 0.6) and a single exponent is presented in Fig. 6-2. It is obvious that a stretch exponent as low as 0.2 is required to generate low onset temperature and broad distribution. However, the same set of parameter cannot simulate the heat capacity curve for a glass formed by slow cooling.

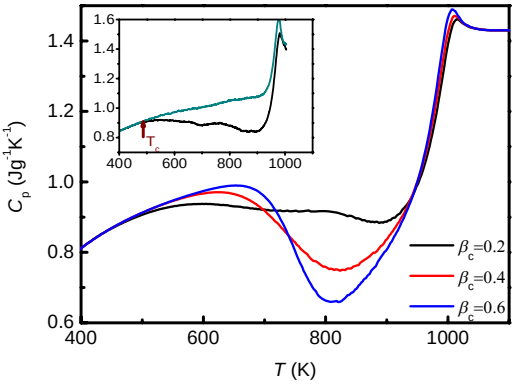

Figure 6-2. Heat capacity simulation by the CRF function with constant stretching exponent 0.2, 0.4 and 0.6. The inset shows the measured heat capacity of hyperquenched fiber.

According to the enthalpy recovery experiments we did for basalt fibers in chapter 5, it has been noted that the stretching exponent is dependent on fictive temperature distribution. Normally, if the fictive temperature is high, then the fictive temperature distribution is also wide and vice versa. Finally, the higher the fictive temperature is, the wider the distribution will be. This experiment supports the stretching exponent in the CRF is strongly dependent on fictive temperature as the equation proposed in ref. [Hornboell et al, 2010],

$$\beta_c = \frac{B_\beta}{T_f - T_\beta} \quad . \tag{6-2}$$

The two parameters T_β and B_β are fitting parameters when the model is fitted to data and are considered as temperature independent material specific constants.

6.2 Heat capacity simulation of fresh and annealed hyperquenched fiber

As the initial plan for this project, a generalized modeling approach was expected which can simulate the enthalpy recovery of fresh and annealed hyperquenched glass fibers. Here below we will give a detailed example to simulate the enthalpy relaxation of glasses far from equilibrium by the CRF function with the stretching exponent as a function of fictive temperature. From the results showing below, it is clear that we need to do more work to develop a generalized approach that can simulate the structural relaxation of glasses far from equilibrium.

6.2.1 The Stretching exponent

As the slow cooled and hyperquenched glasses are expected to be included in one model, the two parameters in equation (6-2) could be determined by the enthalpy relaxation of hyper quenched glass fiber and a slow cooled one with the same composition. Thus, the enthalpy relaxation can be described by the same parameters for a glass

regardless of cooling rate. In terms of the basalt fibers presented in Chapter 5, β_c is determined by combining the distribution of enthalpy recovery of hyperquenched fiber and a slow cooled one. When the annealing temperature is 623 K, the enthalpy recovery during annealing is limited because of the slow relaxation rate. The stretching exponent for 623 K annealed hyperquenched fibers is 0.112 as shown in Fig. 5-4(c) when the T_f is close to that of the fresh hyperquenched fiber, 1202 K. And the stretching exponent is 3/7 for the long range structural relaxation of a homogeneous glass at T_g = 950 K. Thus, ideally, T_β will be 892 K while B_β is 34.8 K by inputting 1202 K (950K) and 0.112 (3/7=0.43) into equation (6-2).

6.2.2 Determination of all other parameters

Other than the above two parameters T_β and B_β, the relaxation time is calculated by Adam-Gibbs [Adam and Gibbs 1965)] equation in our model,

$$\tau = \tau_0 \exp[\frac{B}{TS_c(T_K, T_f)}] \tag{6-3}$$

where τ_0 is the high temperature limitation of relaxation time, B is a fitting constant, S_c is the configurational entropy as a function of Kauzmann temperature, T_K and the glass structure, which has been simplified as fictive temperature, T_f. These constants could be obtained by fitting with the experimental viscosity and the Maxwell equation that assumes relaxation time proportional to the shear viscosity with the shear modulus as the proportional coefficient. Thus, τ_0 in Eq. (6-3) is on the order of η_∞/G=10^{-3} Pa-s/(30*10^9 Pa) =3*10^{-14}. The configurational entropy S_c is defined as [Adam et al, 1965]

$$S_c = \int_{T_K}^{T_f} \frac{(C_{pl} - C_{pg})}{T} dT \tag{6-4}$$

where C_{pl} and C_{pg} are the heat capacities of liquidus and glassy state. Here T_K is taken as a fitting parameter for viscosity. So far, we have got all of the parameters required in order to do the modeling of heat capacity simulation.

6.2.3 Heat capacity modeling for hyperquenched fiber

The measured heat capacity curves of fresh and annealed hyperquenched basalt fibers were presented in Chapter 5, which have fictive temperatures distributed from 1202 K to 930 K. Here we will perform a systematic simulation of heat capacity curves for the glasses having similar thermal history as the ones in the experiment. In the current model, the thermal histories are all assumed to be linear. The starting temperature is 1350 K when the melting is in the equilibrium liquid state. Then the melts is cooled to 350 K where the cooling rate can be any value, followed by the heating process 20 K/min in DSC measurement. Or the fresh fibers could be subjected to an annealing process, where the heating/cooling rate and dwelling time are all inputs of the model, which will be followed by DSC measurement. The whole thermal history of annealed hyperquenched glass fibers are given in Fig. 6-3. The outputs of the model, other than heat capacity, can be enthalpy (taking enthalpy at 1350 K as a reference), fictive temperature, stretching exponent, etc.

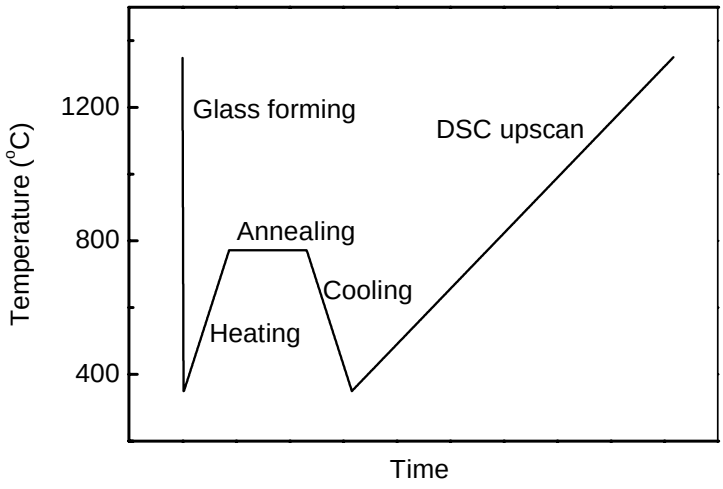

Figure 6-3. Sketched thermal history in the CRF model

The parameters listed in part 6.2.2 are determined by fitting the heat capacity curve of the slow cooled glass. Then the same parameters are transplanted to the fresh and annealed hyperquenched glass fibers. It is clearly shown in Fig. 6-4 that the modeled heat capacity of the fresh hyperquenched fibers is exactly overlapped on the measured heat capacity curve.

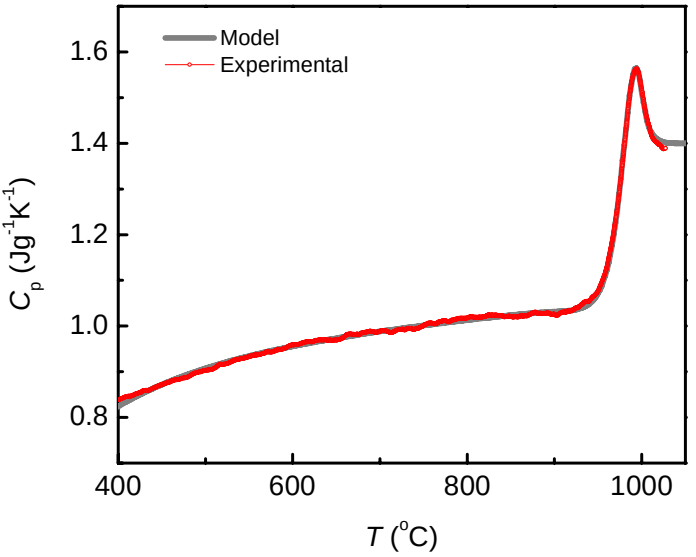

Figure 6-4. The heat capacity curves from model and experiment for slow cooled basalt glass

The modeled and experimental heat capacity of fresh hyperquenched fibers are shown in Fig. 6-5 (a) as well as the experimental and modeled heat capacity curves for the slow cooled glass. As a comparison, we also give the fitted heat capacity curves of hyperquenched NBS-710 glass by TN model from literature in Fig. 5(b). It is obvious that the CRF model captures the onset temperature and high temperature (temperatures around T_g) relaxation very well for the hyperquenched glass fiber comparing with the TN model,

while the distribution at the intermediate temperature from model is not shown as continuous changing as that in the experiment.

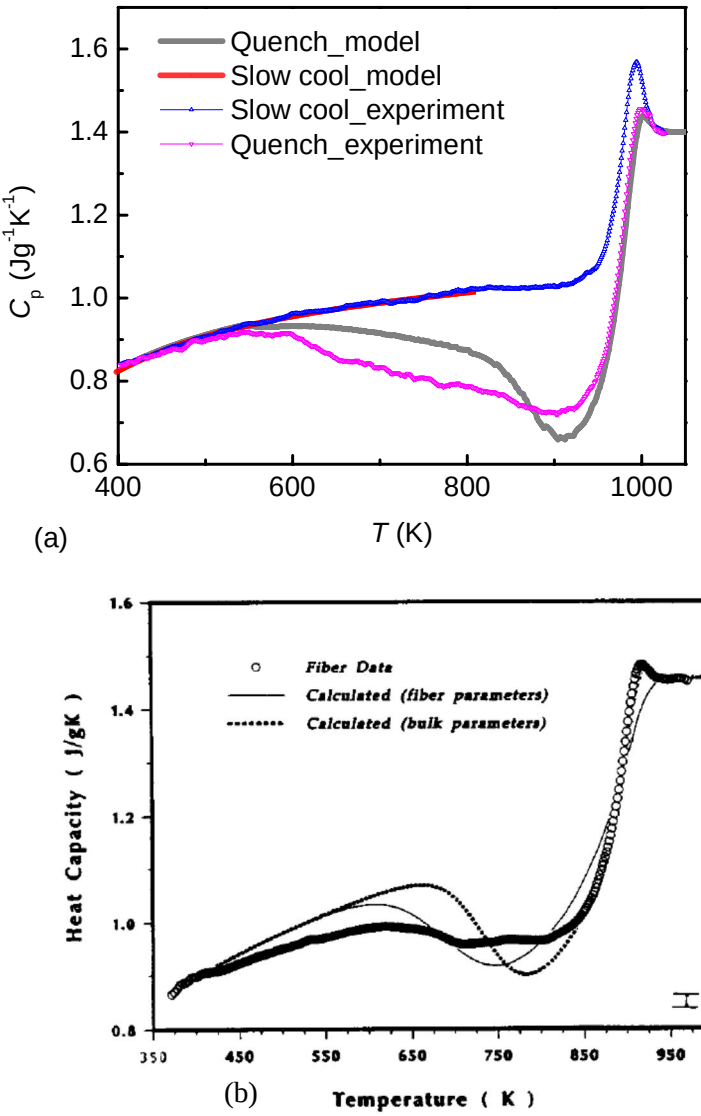

Figure 6-5. (a) The modeled and experimental heat capacity curves in DSC upscan for fresh hyperquenched and slow cooled basalt glass. (b)

Fitted and experimental heat capacity curves of hyperquenched NBS-710 glass fibers from Ref. (Huang and Gupta, 1992)

A three terms combination of the stretching exponent including the above two terms as well as a constant term 0.6 is tested to model the heat capacity curve of the fresh hyperquenched fiber. The two terms combination is shown as model_CRF2 and three terms combination is shown as model_CRF3 in Fig. 6-6. The overall performance of a three terms combination is better than that of the two terms combination. However, it does not show significant improvement in the intermediate temperature range. Further work needs to be performed to test whether a three terms combination could agree better over two terms combination and further probe the physical mechanism. Therefore, the modeling of the annealed hyperquenched glasses will still be performed by using the composite stretching function.

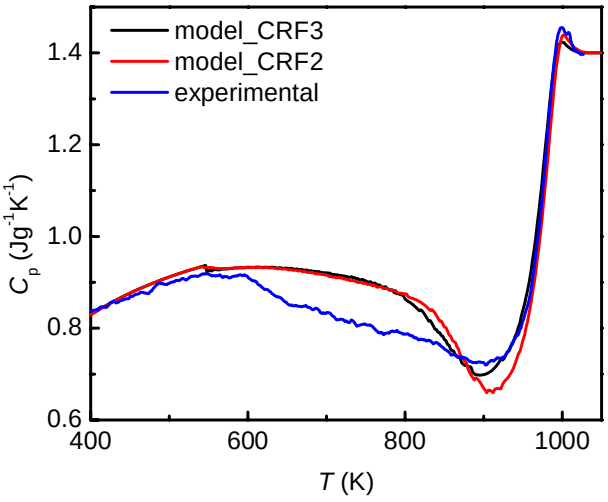

Figure 6-6. Comparison of the performance of three terms combination of stretching exponent vs two terms combination of stretching exponent with the experimental result.

6.2.4 Enthalpy recovery of the annealed hyperquenched fibers

The enthalpy recovery of hyperquenched basalt fibers were experimentally studied at different temperatures. Here we will take 773 K as an example, simulate the heat capacity curves of glasses annealed at 773 K for 5 min, 20 min, 90 min, 6 h, 24 h, and 96 h as shown in Fig. 5-3 (a) by the current model and the parameters obtained for the slow cooled basalt glass.

The experimental heat capacity curves are taken from Fig. 5-3 (a) and inserted in Fig. 6-7(a) for close comparison. The heat capacity difference between the annealed and the fresh hyperquenched fiber are shown in Fig. 6-7(b) with the experimental data as inserts. The features of the experimental heat capacities curves captured by the model are as following : (1) The pre-T_g exotherm peak gets enhanced with increasing annealing time. (2) The heat capacity curves of the annealed fibers are fully overlapped on that from the fresh hyperquenched fiber at the glass transition range, which means the annealing doesn't affect the primary relaxation. However, the enthalpy recovery during annealing is not as fast as the experimental measured values. This reveals that the average relaxation time is not as short as that in the experiment. This could potentially be improved by introducing a new relaxation function into the model.

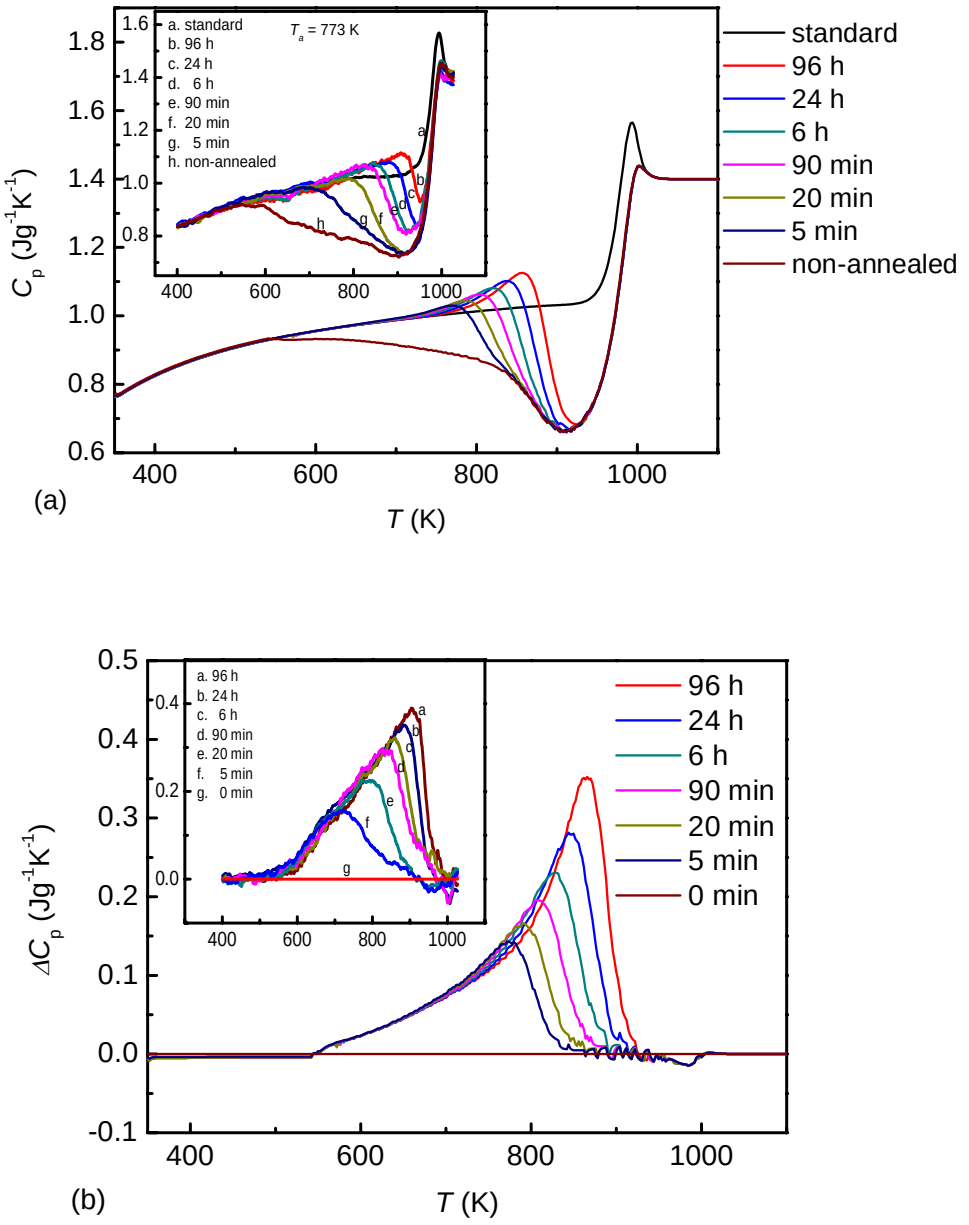

Figure 6-7. (a) Modeled heat capacity curves of basalt fibers annealed at 773K for different duration with the experimental data inserted. (b) Heat

capacity difference for samples annealed at 773 K for different duration minus that of the fresh fiber, the inserted figure is the experimental data.

6.3 Brief summary

We make the effort to generalize the application of TN model for describing the enthalpy relaxation of glasses far from equilibrium. Here the systematic enthalpy recovery study of basalt fibers in Chapter 5 was taken as an example for the performance testing of the composite relaxation function. The modeling of enthalpy relaxation of fresh and annealed basalt fibers reveal that the advantage of composite relaxation function over TN model in terms of: (1) the capability to capture the onset temperature of the pre-T_g exotherm peak; (2) the primary relaxation is not affected by sub-T_g annealing in the studied fictive temperature range; (3) it also reproduces the shallower enthalpy relaxation distribution in the middle temperature range to some extent. However, more work is expected to finalize the application of the composite relaxation function including the utilization of new relaxation function in the non-equilibrium viscosity range and test different composite relaxation function as we did for the two- and three-component stretching exponent.

7. Summary and perspectives

This work contributes to enhancement of basic understanding of glass transition and glass relaxation. The property utilized in the current research is enthalpy which is probed by differential scanning calorimetry (DSC). The study was performed both experimentally and theoretically.

We observe a common glass transition temperature from the heat capacity curves of fresh and annealed glass fibers measured by DSC when identical heating rates are used in the DSC upscan. In the following simulation from temperature modulated differential scanning calorimetry (TMDSC), this point is further demonstrated through generation of the master curve for the reversing heat flow signal, where the glass transition is not dependent on cooling rate prior TMDSC upscan. This phenomenon can be well explained by topological constraint theory, where a glass transition probed by DSC occurs during upscan when the network becomes floppy. The structure of the constraint controlling glass transition is not significantly affected by the cooling rate of glass forming.

Although the glass transition measured by DSC is only dependent on glass composition and the heating rate of the upscan, the glass structure is a function of whole thermal history of a system experienced starting from the equilibrium liquid state. In the glass science community, the glass structure is often simplified to a single fictive temperature. It is noticed that neither of the technical approaches proposed by Moynihan and Yue can be used in description of the heat capacity curves in some of our annealed hyperquenched glass fibers. Based on the identical definition of fictive temperature from Moynihan, we establish a unified approach for the fictive temperature determination for glasses formed through any arbitrary thermal history.

It is obvious that glass relaxation, different from glass transition, is heavily dependent on glass structure. In the study of glass

relaxation, the primary property of focus is still enthalpy, which is measured from DSC/TMDSC. First, we clarify that frequency correction for the non-reversing heat flow is required to get useful information for glass relaxation in TMDSC scan. Second, a systematic study of the enthalpy relaxation is performed for both HQ and AHQ glasses. For the high fictive temperature range from T_g-20 K to 1200 K, the secondary relaxation controls the enthalpy recovery and it is fully decoupled from primary relaxation. We also prove that a single fictive temperature is not sufficient in the analysis of enthalpy recovery in HQ and AHQ basaltic samples, i.e., a distribution of fictive temperatures is required to capture the broad distribution of relaxation times. The broad distribution of activation energies for enthalpy relaxation of HQ and AHQ glasses originates from the high extent of structural heterogeneity in HQ and AHQ glasses where the structural heterogeneity is a direct result of cooling rate. Our experimental results reveal that the stretching exponent in the KWW function varies with the fictive temperature distribution.

According to the experimental results showing variation of stretching exponent with fictive temperature, the composite relaxation function proposed by our group is tested for the enthalpy recovery of annealed basalt fibers. The modeling results reveal that the advantage of composite relaxation function on: (1) the capability to capture the onset temperature of the pre-T_g exotherm peak; (2) the deep overshoot exotherm peak in the glass transition range; (3) it also reproduces the shallower enthalpy relaxation distribution in the middle temperature range to some extent. However, more work is expected to finalize the application of the composite relaxation function including the utilization of new relaxation function in the non-equilibrium viscosity range and test different composite relaxation function as we did for the two- and three-component stretching exponent. In addition, more experimental results and modeling works are needed for testing the composite relaxation function for different glass systems.

References

G. Adam, J. H. Gibbs, “On the temperature dependence of cooperative relaxation properties in glass-forming liquids”, J. Chem. Phys. 43 (1965) 139-146

C. Alba, L. E. Busse and C. A. Angell, “Thermodynamic aspects of the vitrification of toluene, and xylene isomers, and the fragility of liquid hydrocarbons”, J. Chem. Phys. 92 (1990) 617.

P. W. Anderson, “Through the glass lightly”, Science 267 (1995) 1615-1616.

C. A. Angell, ”Relaxation in liquids, polymers and plastic crystals-strong/fragile patterns and problems”, J. Non-Cryst. Solids, 131-133 (1991) 13-31.

C. A. Angell, (1995) “Formation of glasses from liquids and biopolymers”, Science 267 (1995) 1924-1935

C. A. Angell, K. L. Ngai, G. B. McKenna, P. F. McMillan, and S. W. Martin, “Relaxation in glassforming liquids and amorphous solids”, J. Appl. Phys. 88 (2000) 3113-3157.

C. A. Angell, Y. Z. Yue, L. M. Wang, J. R. D. Copley, S. Borick, S. Mossa, “Potential energy, relaxation, vibrational dynamics and the boson peak, of hyperquenched glasses"”, J. Phys.: Cond. Mat. 15 (2003) S1051-S1068

I. Avramov, A. Milchev “Effect of disorder on diffusion and viscosity in condensed systems”, J. Non-Cryst. Solids 104 (1988) 253-260.

I. Avramov, “Influence of disorder on viscosity of undercooled melts”, J. Chem. Phys. 95 (1991) 4439-4443

P. Chen, P. Boolchand, and D. G. Georgiev, “Long term aging of selenide glasses: evidence of sub-T_g endotherms and pre-T_g exotherms”, J. Phys.: Condens. Matter 22 (2010) 065104

K. S. Cole and R. H. Cole, “Dispersion and absorption in dielectric-I Alternating current characteristics” J. Chem. Phys. 9 (1941) 341-352.

K. S. Cole and R. H. Cole, “Dispersion and absorption in dielectric-II diectric current characteristics” J. Chem. Phys. 10 (1942) 98-105.

D. W. Davidson and R. H. Cole, “Dielectric relaxation in glycerine”, J. Chem. Phys. 18 (1950) 1417-1419.

D. W. Davidson and R. H. Cole, “Dielectric relaxation in glycerol, propylene glycol, and n-propanol”, J. Chem. Phys. 19 (1951) 1484-1490.

P. G. Debenedetti, et al. 2001, F. H. Stillinger, “Supercooled liquids and the glass transition”, Nature 410 (2002) 259.

A. Ellison, and I. A. Cornejo, “Glass substrates for liquid crystal displays”, Int. J. Appl. Glass Sci. 1 (2010) 87-103

G. S. Fulcher, ”Analysis of recent measurements of the viscosity of glasses”, J. Am. Ceram. Soc. 8 (1925) 339.

X. J. Guo, J. C. Mauro, M. Potuzak, Y. Z. Yue, “Structural relaxation in annealed hyperquenched basaltic glasses: Insights from calorimetry”, J. Non-Cyst. Solids, 358 (2012) 1356-1361.

P. K. Gupta and J. C. Mauro, “Composition dependence of glass transition temperature and fragility. I. A topological model incorporating temperature-dependent constraints”, J. Chem. Phys. 130 (2009) 094503

S. Havriliak and S. Negami, “A complex plane representation of dielectric and mechanical relaxation processes in some polymers”, Polymer 8 (1967) 161-210.

L. Hornboell, T. Knudsen, Y. Z. Yue and X. J. Guo, “Heterogeneous enthalpy relaxation in glasses far from equilibrium”, Chem. Phys. Lett. 494 (2010) 37-40.

L. Hu, Y. Z. Yue, “Secondary Relaxation Behavior in a Strong Glass”, J. Phys. Chem. B 112 (2008) 9053-9057

L. Hu, Y. Z. Yue, “Secondary Relaxation in Metallic Glass Formers: Its Correlation with the Genuine Johari− Goldstein Relaxation”, J. Phys. Chem. C 113 (2009) 15001-15006.

J. Huang and P. K. Gupta, “Enthalpy relaxation in thin glass fibers”, J. Non-Cryst. Solids, 151(1992) 175-181.

A. Inoue, T. Matsumoto, H. S. Chen, “Enthalpy relaxation behaviour of
metal–metal (Zr–Cu) amorphous alloys upon annealing”, J. Mater. Sci. 20 (1985) 4057-5068

G. P. Johari and D. P. B. Aji, “Time-dependent paths, fictive temperatures and residual entropy of glass”, Philos. Mag. 90 (2010) 4377-4392

J. Kakalios, R. A. Street, W. B. Jackson, “Stretched-exponential relaxation arising from dispersive diffusion of hydrogen in amorphous silicon”, Phys. Rev. Lett. 59 (1987) 1037-1040

R. Kohlrausch, Ann. Phys. (Leipzig) 12 (1847) 393.

R. Kohlrausch, "Theorie des elektrischen rückstandes in der leidner flasche," Ann. Phys. Chem. (Poggendorff), 91 [56-82] (1854) 179-213

A. Kudlik, C. Tschirwitz, T. Blochowicz, S. Benkhof, E. Rossler, “Slow secondary relaxation in simple glass formers”, J. Non-Cryst. Solids 235-237 (1998) 406-411

P. Lunkenheimer, S. Mastner, M. Köhler, and A. Loidl, "Temperature development of glassy α-relaxation dynamics determined by broadband dielectric spectroscopy", Phys. Rev. E 81 (2010) 051504

J. R. Macdonald, J. C. Phillips, "Topological derivation of shape exponents for stretched exponential relaxation", J. Chem. Phys. 122 (2005) 074510

J. C. Mauro, P. K. Gupta, and R. J. Loucks, "Continuously broken ergodicity", J. Chem. Phys. 126, 184511 (2007)

J. C. Mauro, Y. Z. Yue, A. J. Ellison, P. K. Gupta, D. C. Allan, "Viscosity of glass-forming liquids", Proc. Natl Adad. Sci. USA 106 (2009a) 19780

J. C. Mauro, D. C. Allan, M. Potuzak, "Nonequilibrium viscosity of glass", Phys. Rev. B 80 (2009b) 094204

J. C. Mauro, P. K. Gupta, and R. J. Loucks, "Composition dependence of glass transition temperature and fragility. II. A topological model of alkali borate liquids", J. Chem. Phys. 130 (2009c) 234503

J. C. Maxwell, "On the dynamical theory of gases", Phil. Trans. Roy. Soc. Lon. 157 (1867) 49-88

O. V. Mazurin, V. P. Kluyev, S. V. Stolyar, "Temperature dependences of structural relaxation times at constant fictive temperatures in oxide glasses", Glastech. Ber. 56K (1983)1148-1153

O. V. Mazurin, Steklovanie (Glass Transition) Nauka, Leningrad, 1986

M.Micoulaut and G. G. Naumis, "Glass transition temperature variation, cross-linking and structure in network glasses: A Stochastic approach", Europhys. Lett. 47 (5), 568-574

C. T. Moynihan, A. J. Easteal, J. Wilder, and J. Tucker, "Dependence of the glass transition temperature on heating and cooling rate", J. Phys. Chem. 78 (1974) 2673-2677

C. T. Moynihan, A. J. Easteal, M. A. Debolt, J. Tucker, "Dependence of the fictive temperature of glass on cooling rate", J. Am. Ceram. Soc. 59 (1976) 12

C. T. Moynihan, "Correlation between the width of the glass rransition region and the temperature dependence of the viscosity of high-T_g Glasses", J. Am. Ceram. Soc. 76 (1993) 1081

O. S. Narayanaswamy, "A Model of structural relaxation in glass", J. Am. Ceram. Soc. 54 (1971) 491-498

K. L. Ngai, and M. Paluch, "Classification of secondary relaxation in glass-formers based on dynamic properties", J. Chem. Phys. 120 (2004a) 857

K. L. Ngai, S. Capaccioli, "Relation between the activation energy of the Johari-Goldstein β relaxation and T_g of glass formers", Phys. Rev. E 69 (2004b) 031501

J. C. Phillips, "The physics of glass", Phys. Today 35 (1982) 27-33.

J. C. Phillips, "Stretched exponential relaxation in molecular and electronic glasses", Rep. Prog. Phys. 59 (1996) 1133-1207

J. C. Phillips, "Axiomatic theories of ideal stretched exponential relaxation (SER)", J. Non-Cryst. Solids 352 (2006) 4490-4494

M. Potuzak, R. C. Welch, and J. C. Mauro, "Topological origin of stretched exponential relaxation in glass", J. Chem. Phys. 135 (2011) 214502

A. I. Priven, "Calculation of Temperature Dependences of the Viscosity and Volume Relaxation Time for Oxide Glass-Forming

Melts from Chemical Composition and Dilatometric Glass Transition Temperature", Glass Phys. Chem. 27 (2001) 527-542.

G. W. Scherer, *Relaxation in Glass and Composites*; Krieger Publishing: Malabar, FL, 1992

S. L. Simon, G. B. McKenna, "A quantitative analysis of errors in TMDSC in the glass transition region", Thermochimica Acta, 348, 77-89 (2000).

S. L. Simon, "Temperature Modulated DSC: Theory and Application," Thermochimica Acta, 374 (2001) 55-71.

M. M. Smedskjaer, J. C. Mauro, S. Sen, and Y. Z. Yue, "Quantitative Design of Glassy Materials Using Temperature-Dependent Constraint Theory", Chem. Mater. 22 (2010) 5358

M. M. Smedskjaer, J. C. Mauro, and Y. Z. Yue, "Prediction of Glass Hardness Using Temperature-Dependent Constraint Theory", Phys. Rev. Lett. 105 (2010) 115503

M. M. Smedskjaer, J. C. Mauro, R. E. Youngman, C. L. Hogue, M. Potuzak, and Y. Z. Yue, "Topological Principles of Borosilicate Glass Chemistry", J. Phys. Chem. B 115 (2011) 12930

V. G. Tammann, W. Hesse, Z. Anorg. Allg. Chem. 156 (1926) 245-257.

D. Tonchev, S. O. Kasap, " Effect of aging on glass transformation measurements by temperature modulated DSC", Mater. Sci. and Engin. A 328 (2002) 62

A. Q. Tool and C. G. Eichlin, "Variations Caused in the Heating Curves of Glass by Heat Treatment," J. Am. Ceram. Soc. 14[4] (1931) 276-308.

A. Q. Tool, "Relation Between Inelastic Deformability and Thermal Expansion of Glass in its Annealing Range," J. Am. Ceram. Soc., 29 [9] (1946) 240-253

K. D. Vargheese, A. Tandia, J. C. Mauro, “Origin of dynamical heterogeneities in calcium aluminosilicate liquids”, J. Chem. Phys. 132 (2010) 194501

A. K. Varshneya, Fundamentals of Inorganic Glasses, 2nd edition Society of glass technology, Sunderland, 2007.

V. Velikov, S. Borick, and C. A. Angell, “The Glass Transition of Water, Based on Hyperquenching Experiments”, *Science* 294, (2001) 2335-2338

E. Verdonck, K. Schaap, and L. C. Thomas, “Phase Separation of Pharmaceutics”, Int. J. Pharm. 192 (1999) 3-20

H. Vogel, “Das Temperatureabhängigket sgesetz der Viskosität von Flüssigkeiten”, Phys. Zeit. 22 (1921) 645-646.

L. M. Wang, S. Borick, C. A. Angell, “An electrospray technique for hyperquenched glass calorimetry studies: propylene glycol and di-n-butyl phthalate”, J. Non-Cryst. Solids, 353 (2007) 3829-3837.

L. M. Wang, and R. Richert, “Primary and secondary relaxation time dispersions in fragile supercooled liquids”, Phys. Rev. B 76 (2007) 064201

L. M. Wang, M. D. Sun, “”, J. Yanshan Univ. 34 (2010) 471

L. M. Wang, Y. J. Tian, R. P. Liu, and R. Richert, “Calorimetric versus kinetic glass transitions in viscous monohydroxy alcohols”, J. Chem. Phys. 128 (2008) 084503

G. Williams, and D. C. Watts, “Non-symmetrical dielectric relaxation behavior arising from a simple empirical decay function”, Trans. Faraday Soc. 66 (1970) 80-85

L. Wondraczek, H. Behrens, Y. Z. Yue, J. Deubener and G. W. Scherer, “Relaxation and Glass Transition in an Isostatically Compressed Diopside Glass”, *J. Am. Ceram. Soc*. 90 (2007a) 1556-1561

L. Wondraczek, S. Sen, H. Behrens, R. E. Youngman, “Structure-energy map of alkali borosilicate glasses: Effects of pressure and temperature”, Phys. Rev. B 76 (2007b) 014202

Y. Z. Yue, J. deC. Christiansen, and S. L. Jensen, “Determination of the Fictive Temperature for a Hyperquenched Glass”, Chem. Phys. Lett. 357 (2002a) 20-24

Y. Z. Yue, S. L. Jensen, and J. deC. Christiansen, “Physical aging in a hyperquenched glass”, Appl. Phys. Lett. 81 (2002b) 2983-2985

Y. Z. Yue, and C. A. Angell, “Phase transitions in liquids and glasses: their origin, and possible links to switching behavior”, Nature 427 (2004a) 717-721

Y. Z. Yue, R. von der Ohe, and S. L. Jensen, “Fictive Temperature, Cooling Rate, and Viscosity of Glasses”, J. Chem. Phys. 120 (2004b) 8053; *ibid.* Erratum. *J. Chem. Phys.* 121 (2004b) 11508

Y. Z. Yue, L. Wondraczek, H. Behrens and J. Deubener, “Glass transition in an isostatically compressed calcium metaphosphate glass”, *J. Chem. Phys.* 126, 144902 (2007)

Y. Z. Yue, “Characteristic temperature of enthalpy relaxation in glass”, J. Non-Cryst. Solids, 354 (2008) 1112-1118.